United Nations Educational, Scientific and Cultural Organization
GRÓ GTP Geothermal Training Programme Under the auspices of UNESCO

GRÓ GTP, Urðarhvarf 8
IS-203 Reykjavík, Iceland

Reports 2021
Number 6

DELINEATION OF THE ABAYA GEOTHERMAL FIELD, SOUTHERN ETHIOPIA, USING 1D JOINT INVERSION OF MT AND TEM DATA

Eyasu Solomon Abebe
Ethiopian Energy Authority (EEA)
P.O. Box 2554, Addis Ababa
ETHIOPIA
fevijosh@gmail.com, eyasugeothermal@gmail.com, eyab@grogtp.is

ABSTRACT

Surface exploration was carried out in 2018 and in 2019 at Abaya high-enthalpy prospect in Ethiopia with the aim to create a scientific foundation to characterize the geothermal system. The area is located approximately 280 km southeast of Addis Ababa in the Main Ethiopian Rift (MER) and is part of the East African Rift System (EARS) running generally in NNE-SSW direction. A resistivity survey was conducted at the Abaya geothermal prospect area using central loop transient electromagnetic (TEM) and magneto telluric (MT) methods in 2018 and 2019. The TEM method is used to explore the shallow resistivity structure (less than 1 km) using a man-made source signal. In the MT method a natural-source signal is used to image the Earth from several tens of metres to several kilometres' depth. The TEM data are also used for static shift correction of the MT data. Each MT/TEM sounding pair is inverted jointly so that the same 1D resistivity model fits both data sets. 1D means that the resistivity of the Earth only varies with depth. The inversion algorithm applied (Occam inversion) finds the simplest 1D model whose response fits the data. These 1D models are then interpolated and visualized as resistivity maps at different elevations and vertical resistivity cross-sections. The result of the study outlines the resistivity structure and suggests the presence of high-enthalpy geothermal system in Abaya Area. The geothermal system is likely to have a heat source at shallow depth in close vicinity to the tectonically and volcanically active Salewa Dore-Hako rhyolitic complex, which the recent eruptive materials in the area originate from. The results of the resistivity structure are in good agreement with the result of geology, geochemistry, and surface temperature studies.

1. INTRODUCTION

Ethiopia is one of the African countries with huge potential of geothermal resources for direct use and electricity generation applications. The geothermal resource is concentrated in the Main Ethiopian Rift (MER) and in the Afar rift with estimated total potential of 10,000 MWe (Kebede, 2013; Teklemariam and Beyene, 2005).

Even though the country is fully aware of having these high potential geothermal resources, the attempt to start the exploitation of the known resources is still in its infancy except for some areas where hot

water is used for swimming, bathing, and therapeutic purposes. Most geothermal areas are not yet exploited.

Energy is the backbone for development of a country. The progress of industries relies on stable energy resources. Ethiopia has renewable and non-renewable energy resources such as hydropower, solar, wind, geothermal and natural gases. However, the country relies on fossil fuel and imported petroleum and petroleum products. Ethiopia needs to move away from relying too much on fossil fuel and petroleum because of climate change and global warming. Seasonal dependency of hydropower generates the need to develop other stable and reliable energy resources for the country's energy mix. Recently, the country prepared a strategic plan giving geothermal resources development priority right after hydropower (Kebede, 2013; Teklemariam and Beyene, 2005).

There are 24 identified geothermal prospect areas in the Ethiopian rift valley. Eight of them are licenced for independent power producers. Tulu Moye Geothermal and Corbetti Geothermal companies signed power purchase agreement with the Ethiopian government. Tulu Moye Geothermal company has started drilling in the Tulu Moye prospect area to develop a 150 MWe geothermal power plant in two phases. The licence of Alalobeda and Aluto Langano prospect areas have been issued to Ethiopian Electric power. Drilling has started at Aluto Langano to produce up to 70 MWe and upgrade the current geothermal power plant.

Abaya prospect area is one of the potential geothermal fields and is licenced and operated by Reykjavik Geothermal Consulting Co. The company completed surface exploration and planning for detail exploration activities such as test drilling in 2019. They generously provided a sub-set of their resistivity data for the work discussed in this report. The purpose of this project is to acquaint the author with processing and inversion of resistivity data such as MT and TEM data and attempt to delineate the geothermal system.

This report describes the geophysical methods used for geothermal exploration in general and data processing and interpretation of 1D jointly inverted TEM and MT data in particular. The findings of this project describe the subsurface resistivity structure of the Abaya prospect area. Also, data from geochemical studies and geological structures mapped in the area during a surface studies campaign in 2018 and 2019 are integrated with the results of this report.

2. GEOPHYSICAL METHODS IN GEOTHERMAL EXPLORATION

Geophysics is the application of physics to study the Earth, oceans, atmosphere, and near-Earth space. In geophysics, physical properties of rocks or materials such as density, magnetic susceptibility, seismic velocity, electrical conductivity/resistivity, permeability, dielectric permittivity, and chargeability are evaluated and studied to acquire information about the surface and sub-surface.

There are many different geophysical investigation methods. Among these are gravimetric, magnetic, electromagnetic, electrical, seismic, radiometric, and ground penetration radar methods. Geophysical methods can be classified into passive and active methods. Passive geophysical methods detect natural variations in the Earth's crust, such as gravitational, magnetic, and self-potential, while active methods detect the Earth's response to artificially generated signals such as electric currents and seismic waves which are transmitted into the ground to detect characteristics of the Earth's material. Geophysical methods are divided also into direct and indirect or structural methods. Direct methods are directly related to properties of the geothermal resource such as the thermal method and the electrical method. Gravity, magnetic, and seismic methods are indirect methods (Hersir and Björnsson, 1991; Hersir et al., 2022).

Geophysical methods play a key role in geothermal exploration to delineate the geothermal resource, to outline a production field, to locate aquifers or structures that may control aquifers, to site wells, or to assess the general properties of the geothermal system (Georgsson, 2013). A geothermal system consists of five elements: a heat source, a reservoir, a fluid, which is a carrier that transfers the heat, a recharge area and a caprock.

A single geophysical method does not give adequate information to understand the geothermal system. It is important to combine two or more methods for a reasonable interpretation. It is also necessary to include the results of other geoscientific methods such as geology and geochemistry before commencing drilling. The most important methods used in geothermal exploration are described briefly below:

The thermal method is used to measure the temperature of the geothermal system at the surface or in a well. It is directly related to the properties of the geothermal resource. Studies using this method are limited to the surface or a few meters depth, for measurements at greater depth a temperature gradient well is required. The heat exchange mechanisms which are conduction, convection and radiation (almost neglible) are important for the interpretation of the thermal anomalies (Georgsson, 2013).

The gravity method is used to identify lateral density variations in the sub-surface, faults, intrusions and dikes. These changes can give insights into structures at depth which are sometimes related to deep magmatic bodies which are potential heat sources. Gravity surveys can also be used for ground water level and subsidence monitoring in geothermal resource areas.

The magnetic method is applied to map geological structures such as faults and dikes that are often very important in geothermal exploration, especially in low-temperature areas. The result is highly affected when the subsurface temperature exceeds the Curie temperature of around 580°C (Manzella, 2007).

The seismic method can be divided into active and passive seismics. Active seismic measurements give information about density of a formations, porosity and texture, boundaries, discontinuities, and fluid-field zones, and thus, even temperature. In passive seismic methods, natural seismicity is used to delineate active faults and permeable zones. They also give information about the boundary between the brittle and ductile parts of the crust. A shallow brittle-ductile boundary can be an indicator of increased heat in the subsurface (Domra Kana et al., 2015). This method can also be used to monitor seismic activities during production and injection in geothermal sites.

Geophysical well logs are used to study the physical properties of the geothermal system in the vicinity of a well.

Direct current resistivity methods are used to image the resistivity structure in the subsurface and are widely used in geothermal exploration (Hersir and Björnsson, 1991; Hersir et al., 2022).

Electromagnetic methods are used to measure the variations of electrical resistivity in the subsurface of the Earth. The most widely used electromagnetic methods are magneto telluric and time domain electromagnetic methods which are very successful methods in outlining geothermal systems (Pellerin et al., 1996).

2.1 Resistivity of rocks

The resistivity of a material with cross-sectional area A and length L is given by the following equation:

$$\rho = \frac{RA}{L} \tag{1}$$

Where, ρ = Resistivity of the material (Ωm);
R = Resistance (Ω);
L = Length (m); and
A = Cross-sectional area (m^2).

The electric current I is defined by Ohm's law as:

$$I = \frac{\Delta V}{R} \tag{2}$$

Where I = Electric current (A); and
ΔV = Potential difference (V) between the two ends of the conductor with length Δl (m).

From equation (1) and (2) we get:

$$\frac{I}{A} = -\frac{1}{\rho}\frac{\Delta V}{\Delta l} \tag{3}$$

Equation (3) can be written as:

$$j = \frac{E}{\rho} \text{ or } \quad j = \sigma E \tag{4}$$

Where, j = $\frac{I}{A}$ Current density ($A\mathrm{m}^{-2}$);
$E = -\frac{\Delta V}{\Delta l}$ Electric field ($V\mathrm{m}^{-1}$); and
σ = Conductivity of the material ($S\mathrm{m}^{-1}$).

The conductivity σ of a material is defined as the reciprocal of its resistivity ρ.

The parameters that determine the electrical resistivity of rocks are porosity and permeability of the rock, salinity of the water, temperature, water-rock interaction and alteration (Hersir and Björnsson, 1991; Hersir et al., 2022).

Porosity and permeability of the rock

Porosity ϕ is defined as the ratio of pore volume V_v and the total volume of a material V_T:

$$\phi = \frac{V_v}{V_T} \tag{5}$$

Where ρ = Porosity;
V_v = Volume of void space (m^{-3}); and
V_T = Total or bulk volume of the material (m^{-3}).

According to an empirical formula given by Archie (1942), the resistivity and porosity can be related as:

$$\rho = \rho_w a \phi_t^{-n} \tag{6}$$

Where ρ = Bulk (measured) resistivity (Ωm);
ρ_w = Resistivity of the pore fluid (Ωm);
ϕ = Porosity; and
a and n = Empirical constants.

Equation (6) can also be rewritten as:

$$\rho = F\rho_w \tag{7}$$

Where F = $a\ \phi_t^{-n}$ = Formation factor.

If part of the pore space is occupied by air or by natural gas, carbon dioxide or petroleum, Archie's law is modified as follows (Zhdanov and Keller, 1994):

$$\rho = \rho_w\, a\, \phi_t^{-n}\, f^{-c} \tag{8}$$

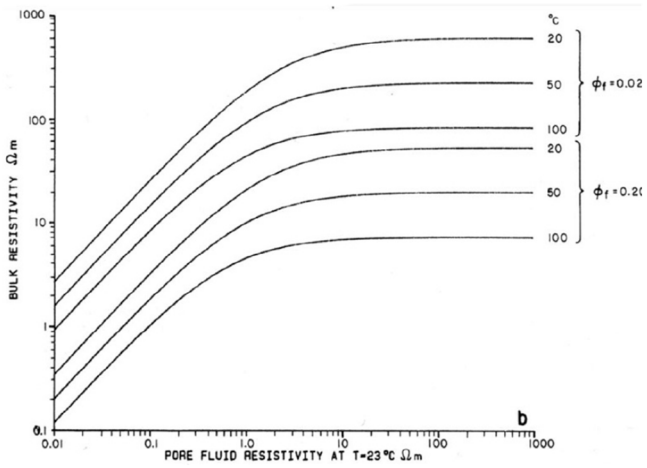

FIGURE 1: Bulk resistivity as a function of pore fluid resistivity for different temperatures and porosities (Flóvenz et al., 1985)

Where f = Fraction of pores containing water of resistivity ρ_w; and c = Empirical constant

Figure 1 illustrates the result of an experiment that shows how the bulk resistivity varies with pore fluid resistivity at different temperatures and porosities. According to the experiment, Archie's law is only valid for conductive solutions with $\rho_w \leq 2$ Ωm (Flóvenz et al., 1985).

Salinity

The bulk resistivity of a rock is largely dominated by the resistivity of the fluid that occupies its pore spaces. An increase in the total amount of dissolved ionsincreases the conductivity substantially.

As shown in Figure 2, the conductivity of a solution depends on mobility and concentration of the ions. This is given by the following equation (Hersir and Björnsson, 1991):

$$\sigma = \frac{1}{\rho} = F(c_1 q_1 m_1 + c^2 q_2 m_2 + \cdots) \tag{9}$$

Where, σ = Conductivity (S/m);
F = Faraday´s number;
(96500 coulombs);
c_i = Concentration of ions;
q_i = Valence of ions; and
m_i = Mobility of different ions.

An increase in the water content and an increase in the total amount of dissolved solids increase the conductivity and are commonly associated with geothermal activity.

Temperature

At moderate temperatures, that is 0-200°C, resistivity of aqueous solutions decreases with increasing temperature as shown in Figure 3. This is due to an increase in ion mobility caused by a decrease in the viscosity of the water. The resistivity of water as a function of temperature can be described by (Dakhnov, 1962:

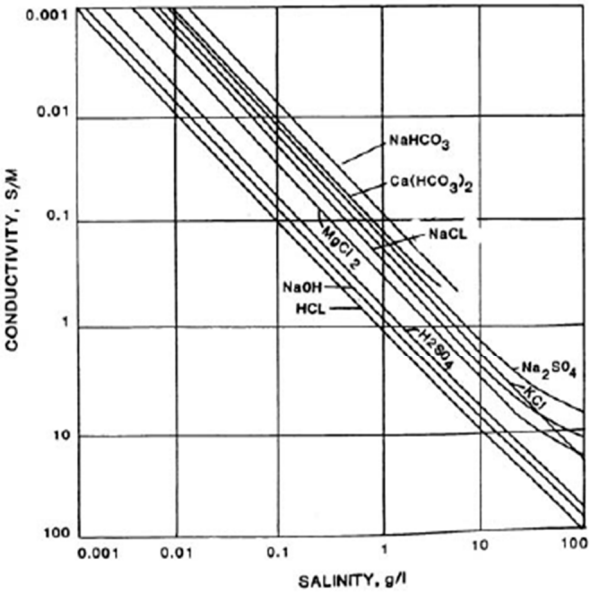

FIGURE 2: Conductivity vs. salinity for different electrolytes (Keller and Frischknecht, 1966)

$$\rho_w = \frac{\rho_{wo}}{1+\alpha(T-T_o)} \quad (10)$$

Where, ρ_w = Resistivity of the fluid at temperature T (Ωm);
ρ_{wo} = Resistivity of the fluid at temperature T_o (Ωm); and
α = Temperature dependent coefficient $(°C)^{-1}$.

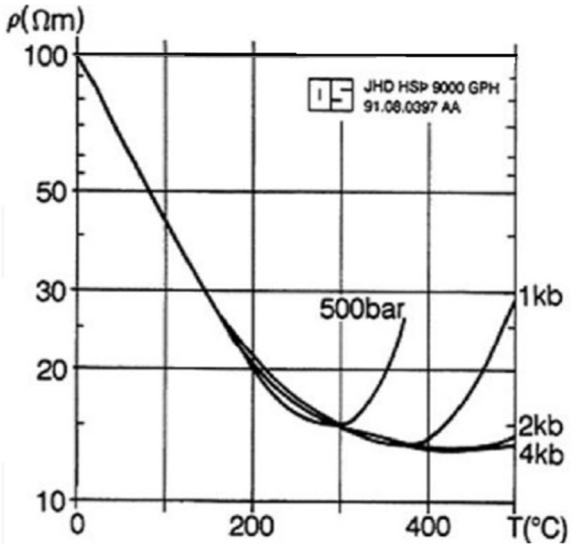

FIGURE 3: Electrical resistivity as a function of temperature at different pressures (Hersir and Björnsson, 1991) modified from Quist and Marshall, 1968.

At high temperatures, a decrease in the dielectric permittivity of the water results in a decrease in the number of dissociated ions in solution. Above 300°C, fluid resistivity starts to increase (Quist and Marshall, 1968).

Water-rock interaction and interface conduction

The bulk conductivity of the rock is the sum of all conductivities as a result of fluid and rock interaction in the volume. It is expressed by the equation (Hersir and Björnsson, 1991):

$$\sigma = \frac{1}{F}\sigma_w + \sigma_s \quad (11)$$

where σ = Bulk conductivity (S/m);
σ_w = Conductivity of water (S/m);
σ_s = Interface conductivity (S/m); and
F = Formation factor of the rock.

The porosity and the pore structure of the rock determines the interface conductivity of the rocks σ_s.

The relationship between subsurface resistivity, hydrothermal alteration, temperature, and conduction mechanism is summarized in Figure 4. The type of alteration minerals and the chemical composition of the geothermal fluid and temperature are the major factors that affect the alteration process and the type of resulting alteration minerals. For temperature less than 50°C the intensity of alteration is low. Low temperature clay minerals such as zeolites and smectite are formed at temperatures lower than 220°C. Conductivity of rocks increases greatly due to the presence of the conductive smectite (Árnason et al., 2000).

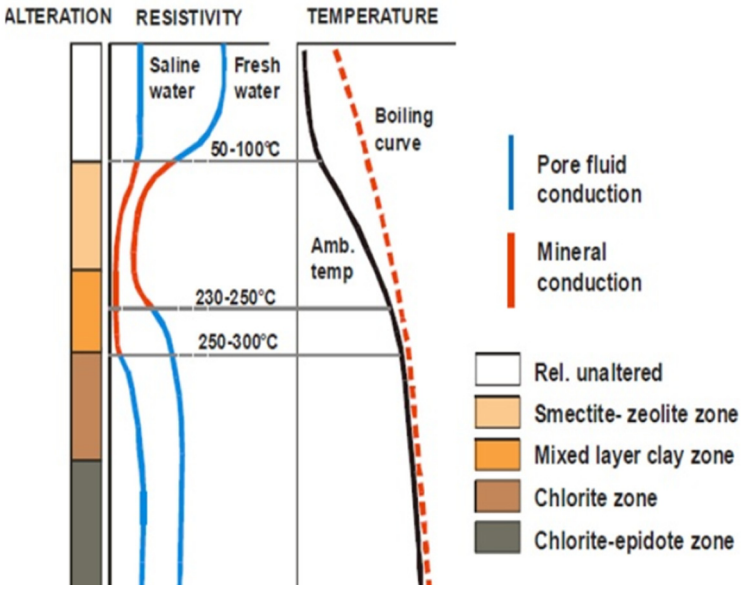

FIGURE 4: A summary of a general resistivity structures of high-temperature area in Iceland ((Flóvenz et al., 2012). Modified from Flóvenz et al., 2005.

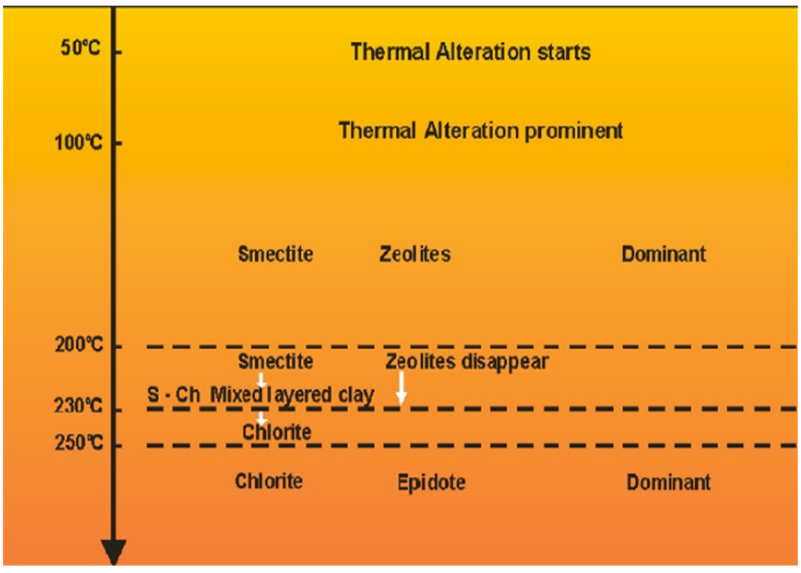

FIGURE 5: Alteration mineralogy and temperature (Hersir and Árnason, 2009)

Figure 5 shows the types of alteration clay minerals at different temperature ranges. In the temperature range from 200°C to about 230°C, the low-temperature zeolites disappear and the smectite is transformed into chlorite in a transition zone, the so-called mixed-layered clay zone, where smectite and chlorite coexist in a mixture. At about 230°C the smectite disappears and chlorite is the dominant mineral, marking the beginning of the chlorite zone. The bulk resistivity increases, since chlorite minerals have cations that are fixed in a crystal lattice, making the mineral resistive.

At still higher temperatures, about 260-270°C, epidote becomes abundant in the so-called chlorite-epidote zone (Árnason et al., 2000).

2.2 Resistivity methods

Resistivity is directly related to properties of the geothermal reservoir such as temperature, alteration, salinity, porosity and permeability (Hersir and Björnsson, 1991; Hersir et al., 2022).

2.2.1 Direct current resistivity methods

In direct current (DC) resistivity methods, an electrical current is injected into the ground through stainless steel current electrodes using a specific electrode arrangement and measuring the change in electric potential at the surface or in boreholes.
The DC resistivity method can be categorized into two methods based on the current and potential electrodes arrangement.

- *Resistivity sounding* is used to determine the vertical variations of the resistivity in the ground. The Schlumberger method or vertical electrical sounding is a common example of a resistivity sounding method. Two or more soundings of this method along a profile can provide information about the lateral variations of resistivity. The depth of investigation depends on the spacing of the electrodes.

  In the Schlumberger method, only the two current electrodes need to be moved, the potential electrodes are only moved stepwise to increase the measured voltage signal. That significantly decreases the time required to acquire data as compared to the Wenner method. A sensitive voltmeter is required for large current electrode spacing. In the Wenner method, all four electrodes are kept at equal distance on a straight line. Increasing that distance increases the depth of penetration.

- *Resistivity profiling* is used to measure the horizontal variation of resistivity with fixed electrode spacing and depth of investigation.

  In the resistivity profiling method, all current and potential electrodes need to be moved so that it may take longer time to acquire data compared to the Schlumberger method. However, it requires a less sensitive voltmeter.

2.2.2 TEM method

A magnetic field of known strength is built up by transmitting a constant current into a loop (Figure 6). The current is then abruptly turned off. The decaying magnetic field induces an electrical current in the ground. The current distribution in the ground induces a secondary magnetic field decaying with time. The decaying rate of the secondary magnetic field is monitored by measuring the voltage induced in the receiver coil at the centre of the transmitter loop. The current distribution and the decay rate of the secondary magnetic field depend on the resistivity structure of the Earth. The induced voltage as a function of time after the current in the transmitter loop is turned off can, therefore, be interpreted in terms of a subsurface resistivity structure (Árnason, 1989). In a central-loop TEM configuration, the induced voltage in a receiver coil (in the frequency domain) on top of a homogeneous Earth is given by (Árnason 1989):

$$V_c\,(\mathrm{r},\mathrm{t}) = I_0 \frac{C_c(\mu_o \sigma r^2)^{3/2}}{10\pi^{1/2} t^{5/2}} \qquad (12)$$

Where $c_c = A_r n_r A_s n_s \frac{\mu_o}{2\pi r^3}$;
A_r = Cross-sectional area of the receiver coil (m2);
N_r = Number of windings in the coil;
μ_o = Magnetic permeability in vacuum (H/m);
A_s = Cross-sectional area of the transmitter loop (m2);
N_s = Number of windings in the loop;
t = elapsed time after the transmitter current is turned off (s);
r = radius of the transmitter loop (m); and
I_0 = Transmitted current.

This shows that the transient voltage is proportional to $\sigma^{3/2}$ and decreases with time as $t^{-5/2}$.
From equation (12) with $\rho = \frac{1}{\sigma}$ the late time apparent resistivity of the central-loop TEM configuration is given by:

$$\rho_a(r,t) = \frac{\mu_o}{4\pi}\left(\frac{2\mu_o A_r n_r A_s n_s I_o}{5t^{5/2}\, V(r,t)}\right)^{2/3} \tag{13}$$

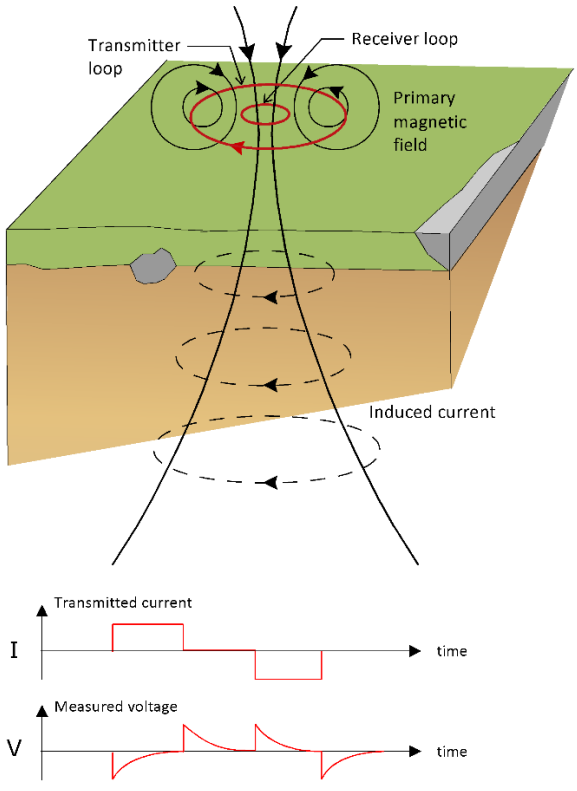

FIGURE 6: Central-loop TEM configuration (Flóvenz et al., 2012)

The central-loop TEM sounding method has several advantages over conventional DC sounding methods (Árnason, 1989). No current is injected into the ground in TEM method so that it avoids the challenge to inject the current in areas where the surface is highly resistive (Árnason, 1989) and the measured signal on the surface is a decaying magnetic field, rather than an electric field, which is not affected by local resistivity conditions at the receiver site (Sternberg et al., 1988). Resistivity inhomogeneities at the receiver site cause severe problems in DC and MT soundings (Árnason, 1984). TEM is preferable for depth sounding surveys in rough topography areas where wire extensions for the DC method are challenging, and it is less sensitive to lateral resistivity variations than the DC methods. In addition, one-dimensional inversion is better justified in the interpretation of central-loop TEM soundings than in DC soundings.

2.2.3 MT method

The MT method is a passive electromagnetic method that uses the natural magnetic field of the Earth. Variations of the magnetic field induce currents in the conductive ground. In the MT method, the orthogonal electric field (Ex and Ey) and magnetic field (Hx, Hy and Hz) are measured to determine the conductivity structure of the Earth at depths ranging from a few tens of meters to several kilometres (Simpson and Bahr, 2005). For a simple resistivity structure and noise free data the electrical field is coherent with its orthogonal source magnetic field, i.e., Ex correlates with Hy, and Ey with Hx, while in the real world this relation depends on the Earth's resistivity structure.

Interaction between the solar wind and the ionosphere generates an electromagnetic field at frequencies of less than 1 Hz (Figure 7). This source of the electromagnetic field helps to acquire deeper resistivity information of the study area. Thunderstorm activity causes magnetic fields at frequencies above 1 Hz and provides information about the resistivity structure of the Earth at shallow depth.

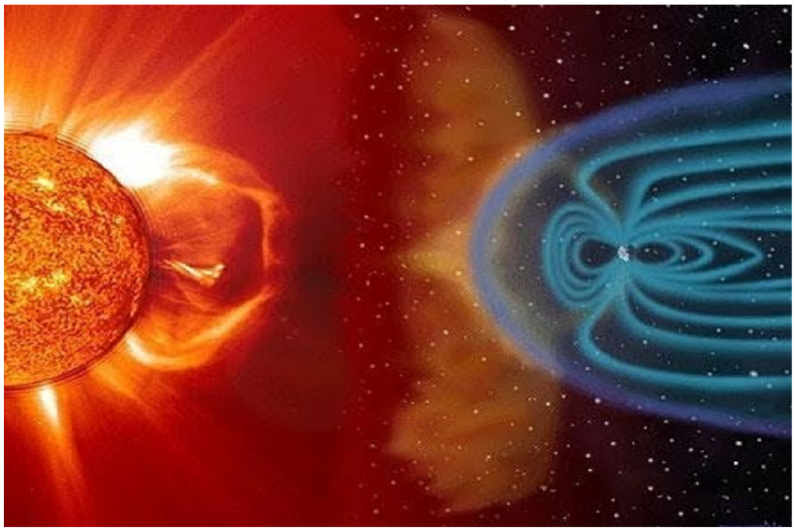

FIGURE 7: Interaction of solar wind with magnetic with magnetosphere (SOHO, 2010)

These natural phenomena create strong MT source signals over the entire frequency spectrum. The depth to which electromagnetic waves penetrate a uniform ground of resistivity ρ and are attenuated to e^{-1} of their amplitudes at the surface of the earth is called the skin depth δ.

The skin depth δ is defined as:

$$\delta = \left(\frac{2}{\omega\mu\sigma}\right)^{1/2} \tag{14}$$

Where, ω = angular frequency;
μ = relative permeability of the conductor; and
σ = conductivity of the Earth.

Therefore, the skin-depth increases with lower frequency and is larger for a resistive Earth.

The electric field and the magnetic field can be related by a transfer function through an impedance tensor **Z** given by (Dobrin, 1988):

$$\mathbf{E} = \mathbf{ZH} \quad (15)$$

Where **E**, **H** and **Z** are functions of frequency.

In a Cartesian coordinate system (*x*, *y*) Equation (15) can be expressed by the matrix equation:

$$\begin{pmatrix} E_x \\ E_y \end{pmatrix} = \begin{pmatrix} Z_{xx} & Z_{xy} \\ Z_{yx} & Z_{yy} \end{pmatrix} \begin{pmatrix} H_x \\ H_y \end{pmatrix} \quad (16)$$

The impedance of a homogeneous ground is given by (Zhdanov and Keller, 1994):

$$Z = \begin{pmatrix} 0 & Z \\ -Z & 0 \end{pmatrix};$$

$$Z = \frac{E_x}{H_y} = -\frac{E_y}{H_x} = \frac{i\omega\mu}{k} \quad (17)$$

Where Z = Impedance of the medium (V/A or Ω);
ω = Angular frequency (Hz);
μ = Magnetic permeability (H/m);
σ = Conductivity of the medium (S/m);
E_x = Electric field strength (V/m) in *x* direction;
H_y = Magnetic Field strength (T) in y direction;
$k = \sqrt{i\omega\mu(\sigma + i\omega\varepsilon)}$ wave propagation number; and
ε = Dielectric permittivity (C/ V m).

.

The wave propagation number can be simplified as:

$$k^2 = i\omega\mu\sigma \text{ and Z reduces to } Z = \sqrt{\omega\mu\rho} \cdot e^{-i\pi/4} \quad (18)$$

Z is complex, composed of both real and imaginary parts. In Equation (18), $\pi/4 = 45°$ is the phase difference between E_x and H_y with E_x leading (Figure 8). For a non-homogeneous Earth, the apparent resistivity, ρ_a is defined as:

$$\rho_a = \frac{1}{\mu\omega}|Z|^2 \quad (19)$$

Similarly, the apparent phase of a complex impedance function is defined as:

$$\phi = tan^{-1}\left(\frac{Im(Z)}{Re(Z)}\right) = \arg(Z) \quad (20)$$

For a 1-D Earth, where conductivity varies only with depth, the diagonal elements of the impedance tensor Z_{xx} and Z_{yy} are zero. The off- diagonal components are equal in magnitude, but have opposite signs, i.e $Z_{xy} = -Z_{yx}$. For a 2-D Earth, in which conductivity varies along one of the principal horizontal direction as well as with depth, Z_{xx} and Z_{yy} are equal in magnitude but have opposite signs and Z_{xy} and Z_{yx} are not equal. For a 2-D Earth with the x and y direction aligned along the electromagnetic strike, Z_{xx} and Z_{yy} are equal to zero. In the general, 3-D case, all four components of the impedance tensorare non-zero. For a 2-D Earth after rotation to a principle (strike) direction, the two apparent resistivities based on the off diagonal impedances are given by:

$$\rho_{xy} = \frac{1}{\omega\mu}\left|Z_{xy}\right|^2 \; and \quad \rho_{yx} = \frac{1}{\omega\mu}\left|Z_{yx}\right|^2 \tag{21}$$

The effective impedance tensor Z_{eff} is rotationally invariant and is given by the determinant of the impedance matrix in equation (18):

$$Z_{eff} = (\, Z_{xx}\, Z_{yy} - Z_{xy}\, Z_{yx}\,)^{1/2} \tag{22}$$

Therefore,

$$\rho_{eff} = \frac{1}{\omega\mu}(Z_{eff})^2 \text{ and } \phi_{eff} = \arg(Z_{eff}) \tag{23}$$

Static shift

The static shift phenomenon is caused by local near-surface resistivity inhomogeneities which distort the electric field, independent of period. This is known for resistivity methods where the electric field is measured on the surface, like in the MT and DC soundings. The apparent resistivity values are shifted by an unknown multiplier (a shift on logarithmic scale), however, it does not affect the phase. The TEM soundings do not suffer the static shift problem because they measure magnetic induction in a receiver coil (or loop). Therefore, TEM data can be used to correct the MT data as proposed by several authors (Sternberg et al., 1988; Pellerin and Hohmann, 1990). The static shift factor can be extracted through a joint interpretation of TEM and MT soundings that were made at the same location. In volcanic areas near-surface inhomogeneities are common and it is therefore important to use TEM to correct for the static shift. Abaya prospect is one of such areas. The TEM remedies the static shift if the shallow resistivity structure is horizontally layered. This is not the case if there is rough topography at the measurement site or if there is horizontal variation in the resistivity structure close to the surface.

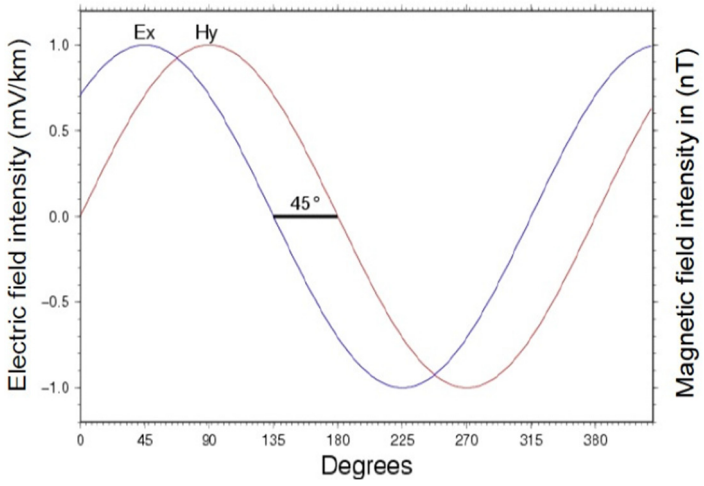

FIGURE 8: Homogeneous half-space response of electric and magnetic field intensity

Strike analyses

The direction along which the conductivity is constant is known as the geoelectric strike, or Zstrike. The geoelectric strike direction can be determined by strike analysis of MT data by finding the angle of rotation for which $\left|Z_{xx}\right|^2 + \left|Z_{yy}\right|^2$ is minimized.

Strike analysis gives valuable information about the general distribution of resistivity in the study area, the boundary of the geothermal reservoir, characteristics of fractures and faults at different depth levels and geodynamic processes in the Earth.

According to Swift (1967), before starting two-dimensional analysis of MT data the impedance tensor needs to be rotated by an angle such that the magnitude of the sum of the absolute value squared of the two diagonal elements is minimized. There is, however, a 90° ambiguity in the Zstrike

The skew S is a measure of the dimensionality of the structure:

$$S = \frac{Z_{xx}+Z_{yy}}{Z_{xy}+Z_{yx}} \quad (24)$$

For a 3D-Earth, the value of S is large but the value is zero and close to zero for a 1D- Earth and a 2D-Earth, respectively.

Wiese (1962) and Parkinson (1983) explain the strike direction in a different way as shown in equation 25:

$$H_z = W_{zx}H_x + W_{zy}H_y \quad (25)$$

Where $[W_{zx}W_{zy}] = W$ is the Wiese-Parkinson matrix, also known as the Tipper. H_x, H_y and H_z are the components of the magnetic field in x, y and z direction, respectively. The matrix W gives information about the symmetry of the excess currents caused by the horizontal distribution of the resistivity.

There is no induced current in vertical direction for a 1D Earth, therefore W=0. For a 2D-Earth, the rotation of the coordinates system places the x-axis in the strike direction (also known as T-strike) to minimize H_x and hence minimizing | W_{zx}|=0 which in turn implies maximization of $|W_{zy}|$. The rotation impedance does not affect the T-strike, therefore, there is no 90° ambiguity in the T-strike.

3. ABAYA PROSPECT AREA

The Abaya project area exhibits some of the most prominent surface manifestations and has thus received exploration attention which have led to encouraging results.

3.1 Regional geological and tectonic settings

The East African Rift System (EARS) is about 6,500 km in length and extends from the Red Sea in the north to Mozambique in the south. According to Corti (2009), the EARS is an intra-continental rift system caused by normal faulting and basalt eruptions are distributed widely in trap series.

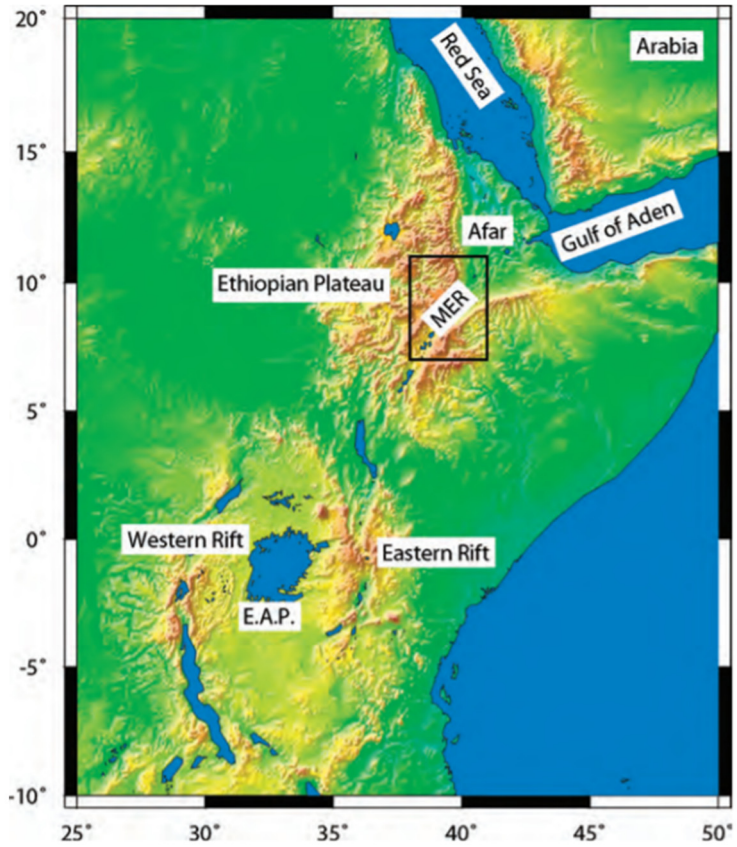

FIGURE 9: East African Rift System (Maguire et al., 2006)

The East African Rift System has two branches namely the Eastern and Western Rift as shown in Figure 9. The Ethiopian Rift system is located in the Eastern branch and includes the Main Ethiopian Rift and the Afar depression. All geothermal prospect areas are located along the Main Ethiopian Rift as shown in Figure 10. MER is an oblique rift, NE-SW trending and formed by E-W extension between the Nubia and Somalia plates via magmatic intrusions and tectonic faulting (Ebinger, 2005; Corti, 2009; Corti et al., 2013).

Geodetic and seismic data show that the current E-W extension rate is about 4-6 mm per year (Bendick et al., 2006; Keir et al., 2006; Stamps et al., 2008).

The Ethiopian rift system gives a complete picture of how rift morphology develops through time, from fault-dominated in the southern MER to magma-dominated in the northern MER (Corti, 2009). Active faulting and volcanic activities are mostly localized along N-S trending fault systems like the Wonji fault belt, which is located in the rift floor (Kazmin, 1980). The Wonji fault system Belt (WFB) is characterized by active extension fractures and normal faults which are related to fissural and central volcanic activity.

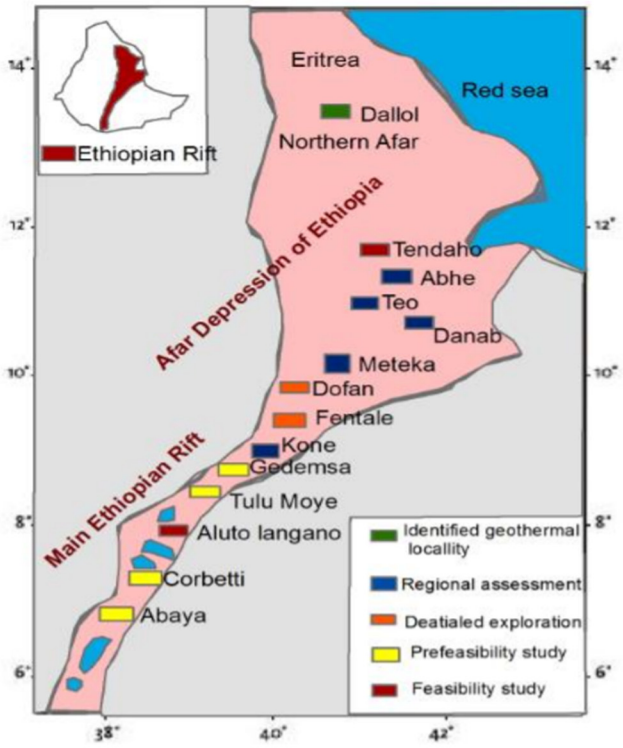

FIGURE 10: Geothermal prospect Areas in Main Ethiopian Rift (Teklemariam, 2005)

3.2 Local geological and tectonic setting of Abaya Geothermal prospect

The Abaya area is located in the South Main Ethiopian Rift (SMER) which extends from Lake Awassa in the north into the Ganjuli Basin in the south as shown Figure 11. The SMER is thought to be less evolved in comparison to the Central and Northern MER (Corti et al., 2013). The tectonic history of the SMER began in the late Miocene with regional extensional tectonics and subsidence. This was followed in the Pliocene by rift-margin rhyolitic volcanism, producing extensive ignimbrite successions and trachytic volcanism in the rift-shoulders. In the SMER, shallow crustal magma chambers which feed the axial volcanic complexes provide the heat for the hydrothermal system. This hydrothermal system resides in the Tertiary volcanic succession, with lacustrine and volcaniclastic infill sediments acting as a caprock (Chernet, 2011). The area is characterized by the absence of a major rift escarpment as might be expected from a rift margin setting, and instead the topographic transition is gentle between the rift floor and plateau (Minissale et al., 2017).

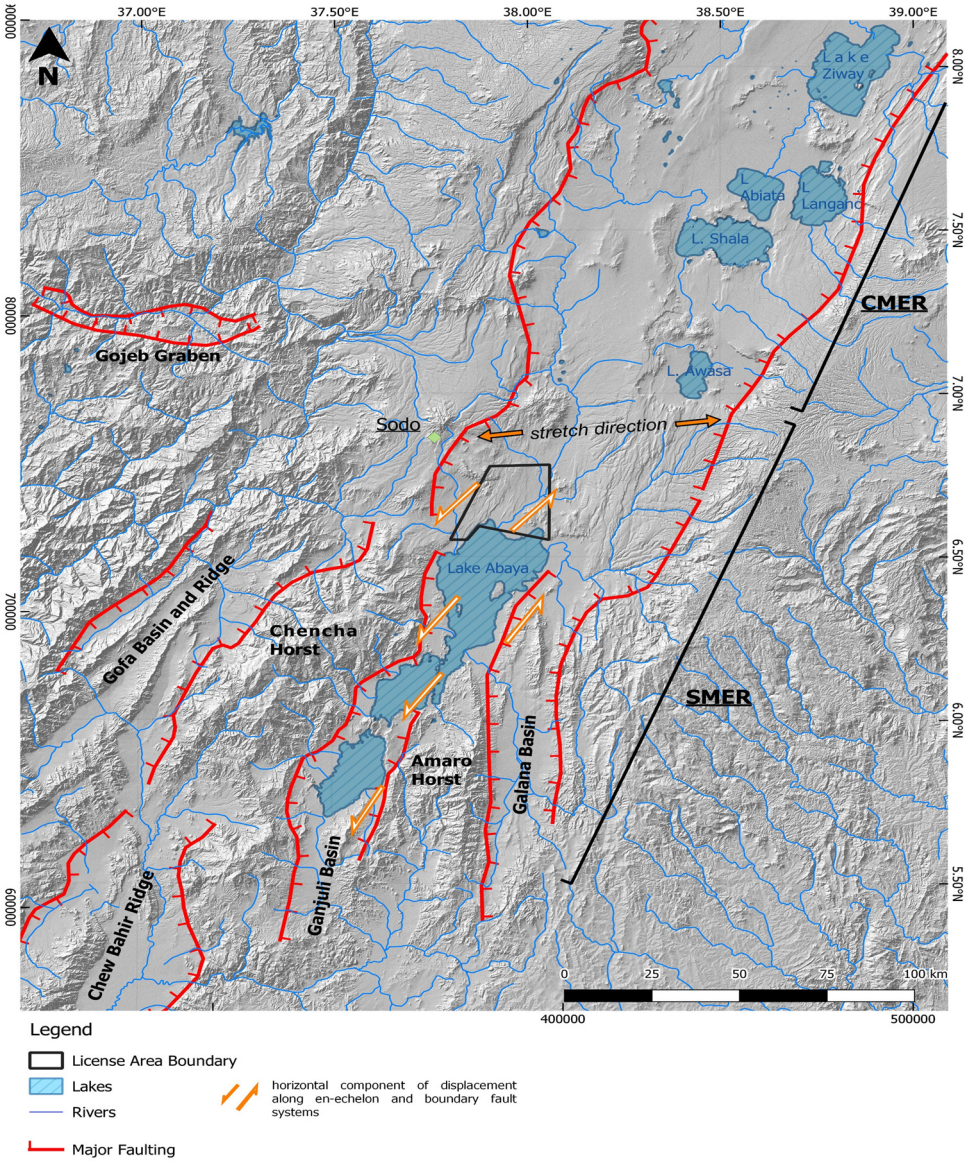

FIGURE 11: Tectonic overview of the SMER where the Abaya geothermal concession is located (black polygon). The main tectonic features show that the SMER divides into three main segments: Gofa Basin and Ridge in the west and Ganjuli and Galana Basins in the east. Modified from Reykjavik Geothermal.

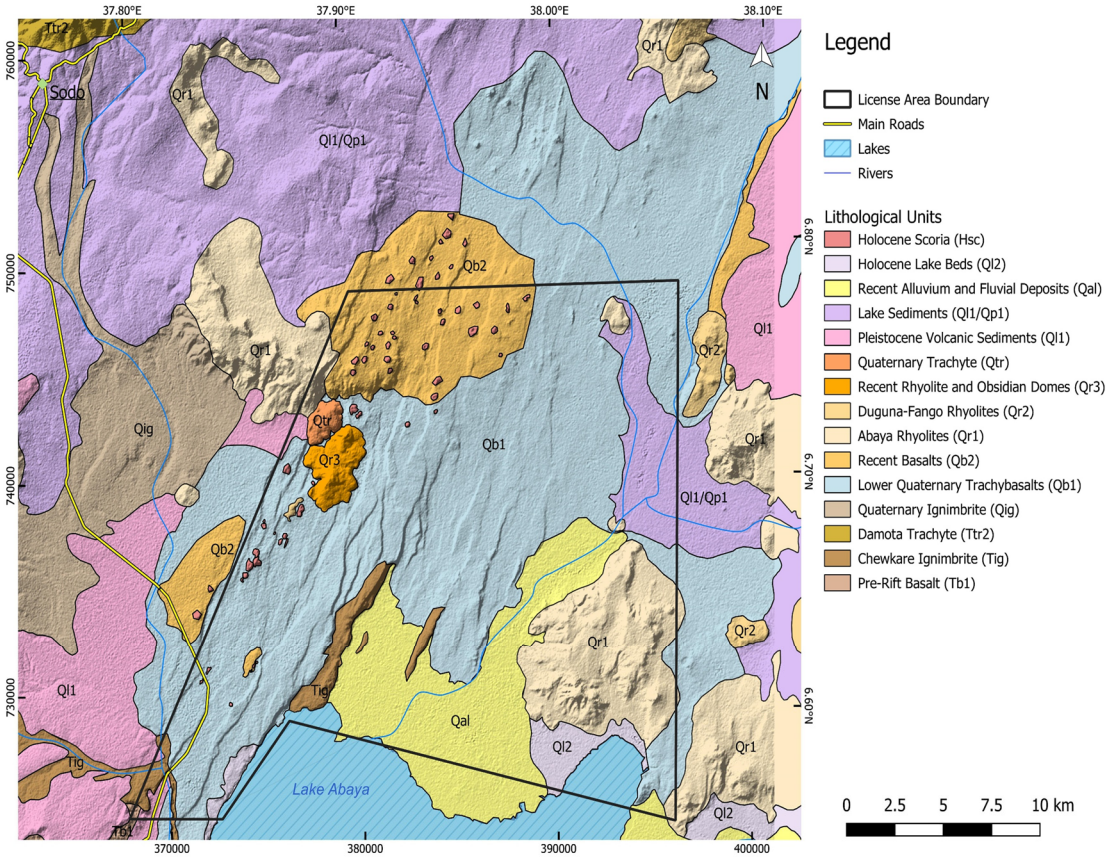

FIGURE 12: Geological map of Abaya project area, modified from Reykjavik Geothermal. The Abaya geothermal concession is indicted by the black polygon.

The main geological features in the geothermal area presented in the map in Figure 12 are:

- Alluvial cover: Holocene to present, found around the rift valley
- The Salewa Dore – Hako Complex: a rhyolitic complex built in several eruptive periods during the Holocene
- The Salewa Dore – Hako Graben: a post Obitcha Caldera faulting, cutting through the Obitcha caldera wall with an NNE-SSW faulting direction
- Numerous scoria cones: aligned in the dominant fault direction of the SD-H Graben, the main source of the recent basaltic lavas
- Recent basaltic lavas: syn-rift
- The Obitcha Caldera: a Pleistocene formation

3.3 Location of the project

The study area in this project is located north of Abaya Lake in Southern Nations Nationality Peoples Regions of Ethiopia, approximately 280 km southwest of Addis Ababa and 30 km Southeast of Sodo as shown in Figure 13. The prospect area covers 514 km^2 and is the concession area of Reykjavik Geothermal (RG).

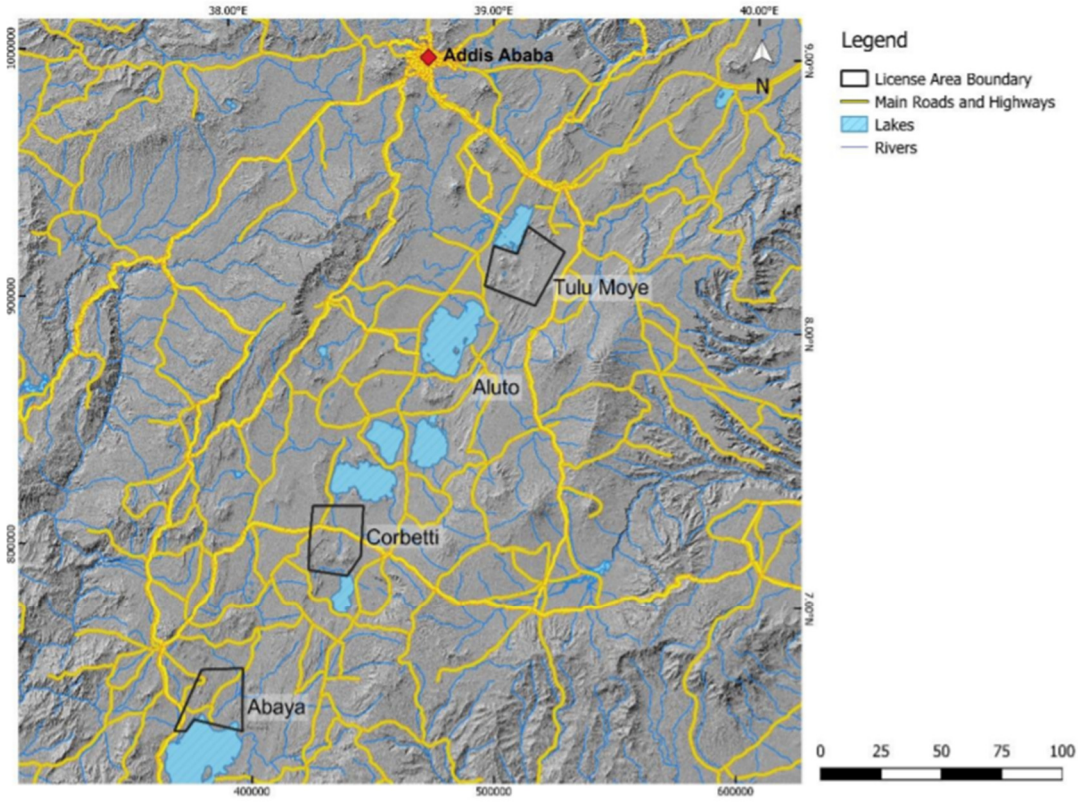

FIGURE 13: Location map of the Abaya Corbetti and Tulu Moye project areas, modified from Reykjavik Geothermal

3.4 Geothermal manifestations

The geothermal surface manifestations at Abaya geothermal project area, are surface alteration, hot springs, steaming ground and fumaroles. Most geothermal manifestations are aligned along the NNE-SSW trending Abaya fault as shown in Figure 14.

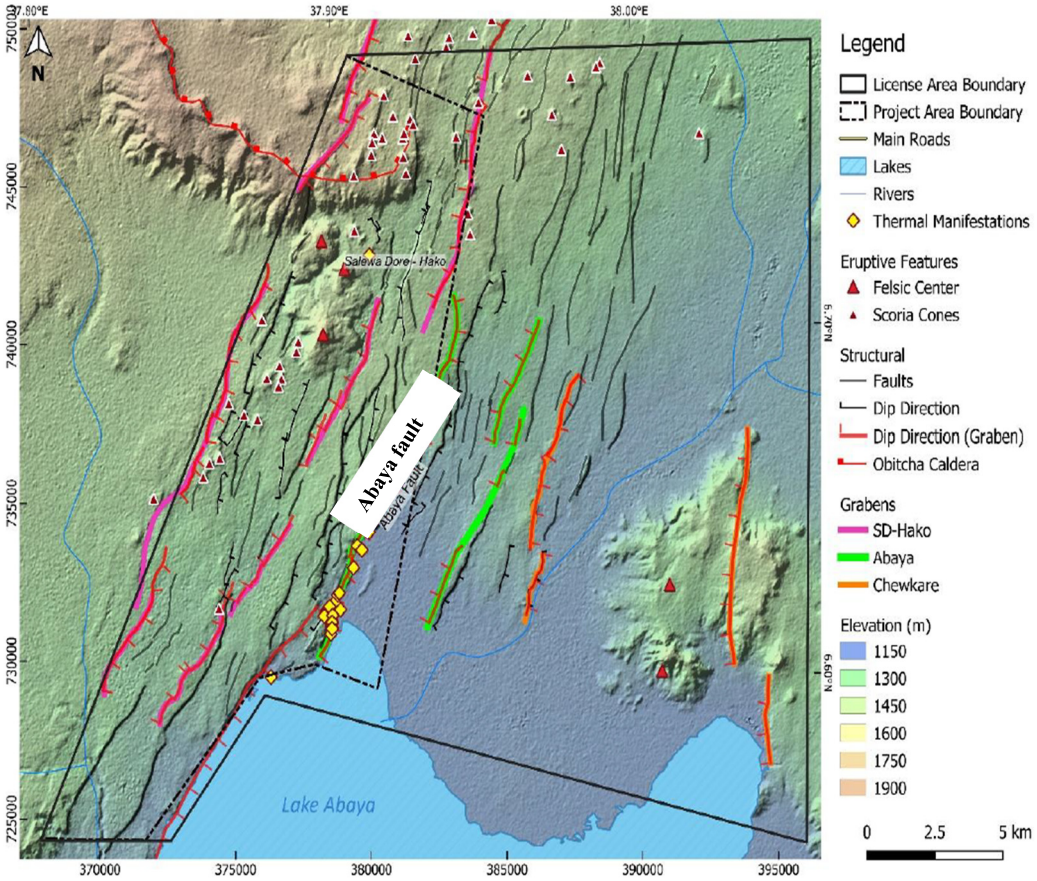

FIGURE 14: Geothermal surface manifestation at Abaya, modified from Reykjavik Geothermal

3.5 Previous studies

The geothermal exploration in MER began in 1969, carried out by the Ethiopian government and the United Nations Development Program (UNDP). The activities included geology, geochemistry, and hydrology studies of the hot springs in the East African Rift (Gebregziabher, 1997).

Following the reconnaissance survey from 1969 – 1973 conducted by UNDP and the Ethiopian government, further detailed geological, geochemical, and geophysical surveys were carried out by the Ethiopian Institute of Geological survey in the Abaya, Corbetti and Shalla areas. These studies indicate the existence of a heat sources associated with a shallow magma chamber beneath the Abaya and Corbetti fields. Based on the available data the area of the lakes district Rift was given priority for further exploration activities.

In 1980, the technical review committee (with the participation of United Nations experts) selected the highest priority areas in addition to the Aluto Langano geothermal field. The Corbetti and Lake Abaya geothermal areas were recommended as second and third priority, respectively (Gebregziabher, 1997). Reykjavik Geothermal carried out surface exploration in the Abaya geothermal area from 2018 until June 2019. The work included the digitization of existing geological maps, geological field work,

sampling of geochemical fluids, gas and water, soil gas flux and temperature surveying, structural mapping, petrological sampling, and resistivity surveying covering an area greater than 70 km^2.

4. RESISTIVITY IN THE ABAYA PROJECT AREA

4.1 MT and TEM data

A resistivity survey was used to identify and delineate the potential geothermal system in the Abaya area. The resistivity pattern generally observed in high enthalpy geothermal systems is a sequence of high- low-high resistivity variations with depth. The low resistivity layer is associated with conductive thermal alteration and is often called the "clay cap" layer. Below this layer are different thermal alteration minerals which are resistive. At the interface of the low and high resistivity layers, i.e., the base of the clay cap layer, the expected temperature is around 230°C. However, the temperature could be lower if the system has cooled down – then the alteration structure 'freezes', even though the system has cooled. The resistivity survey aims to identify such a resistivity structure.

A resistivity survey often comprises of two methods, central loop transient electromagnetic (TEM) and magneto telluric (MT). TEM is used to explore the shallow resistivity structure (less than 1 km) using a manmade source signal. The MT method uses a natural source signal. The MT penetration depth is a few tens of metres to a few kilometres. The TEM is also used for static shift correction of the MT data.

Figure 15 shows the location of the MT and TEM soundings. The Northing and Easting are UTM coordinates in kilometres, zone 37 and WGS84 datum. The coordinates of the soundings are given in Appendix 1 (REF).

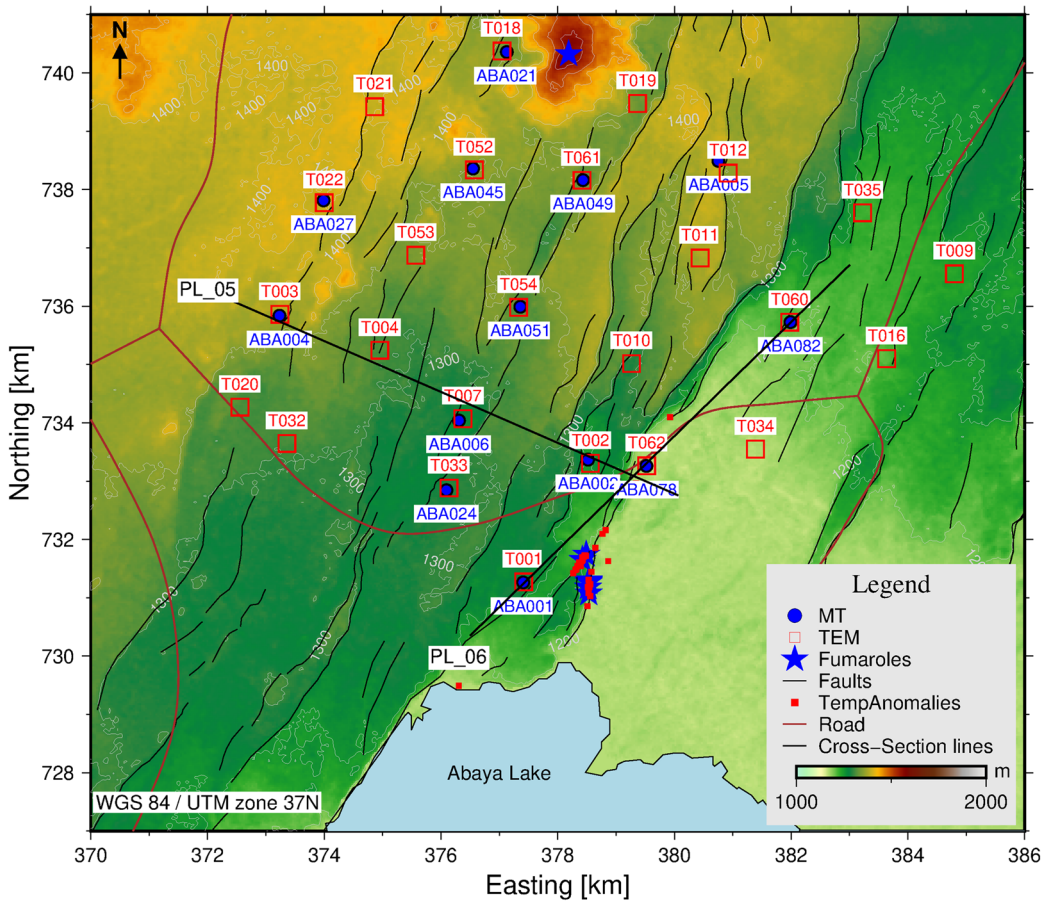

FIGURE 15: Location of MT and TEM soundings.
Red squares are TEM soundings and blue filled circles are MT soundings.
PL 05 and PL 06 show the location of the resistivitv cross sections

The MT/TEM survey was conducted in two separate field surveys, one in November of 2018 and the other in February 2019.

4.1.1 TEM Soundings

The TEM instruments used were of model WTEM-2 made by BTSK/WTSGGEO in China. They consist of a 10 kW current transmitter and a receiver unit. The transmitter and the receiver are synchronized by GPS clocks. The power source is Li-ion batteries, each producing 48 V, 20 Ah and weighing 7 kg each. 1 to 3 batteries were used in series for up to 144 V. For three batteries in series the current is about 36 A in the 200 x 200 metre source loop. Two kinds of receiving loops were used, one has 400 windings over an area of one meter square or an effective area of 400-meter square, the other is a seismic cable of 52 windings and a 100-meter square area (10 x 10 m) or an effective area of 5200-meter square. For part of the survey two instruments were used by two TEM groups. For the conditions in Abaya area and the instrument setup, the depth of penetration of the TEM soundings was generally 300-700 meters.

A total of 88 TEM sounding were measured in the project area. For this project, 26 of these soundings were selected for data processing. All the TEM data and their corresponding 1D interpretations are displayed in Appendix 2 (REF). The TEM data are generally of good quality with times from current turn off ranging from 20 µs to 200 ms. Figure 16 shows an example of two TEM soundings from the project area. The data are displayed as late time apparent resistivity as a function of time from current turn-off. The calculated apparent resistivity would be the ground resistivity if it was homogeneous, i.e., the same resistivity everywhere in the ground. The resistivity is measured in Ωm and is in fact the specific resistivity of the surface. The time from current turn-off is shown in microseconds (µs), the longer this time is the deeper is the penetration depth. In all cases data were sampled at two different frequencies (4 Hz and 1 Hz).

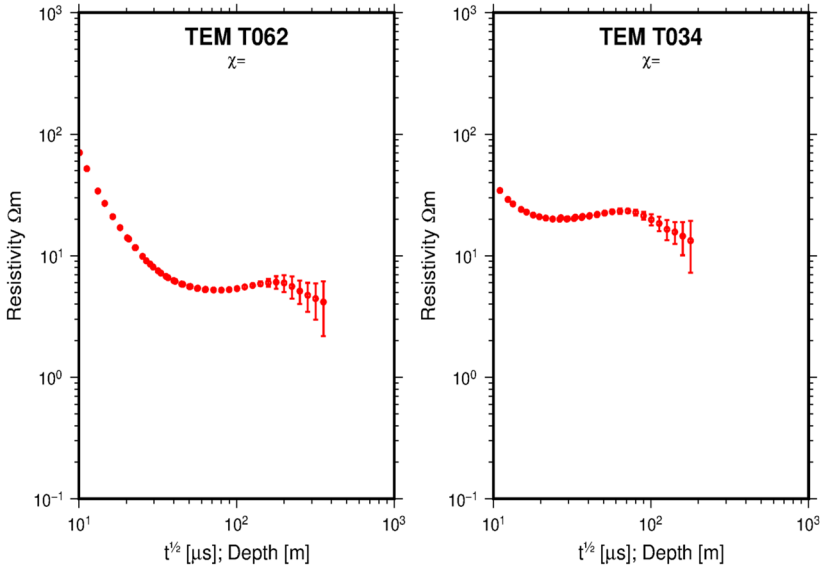

FIGURE 16: Examples of TEM soundings

4.1.2 MT soundings

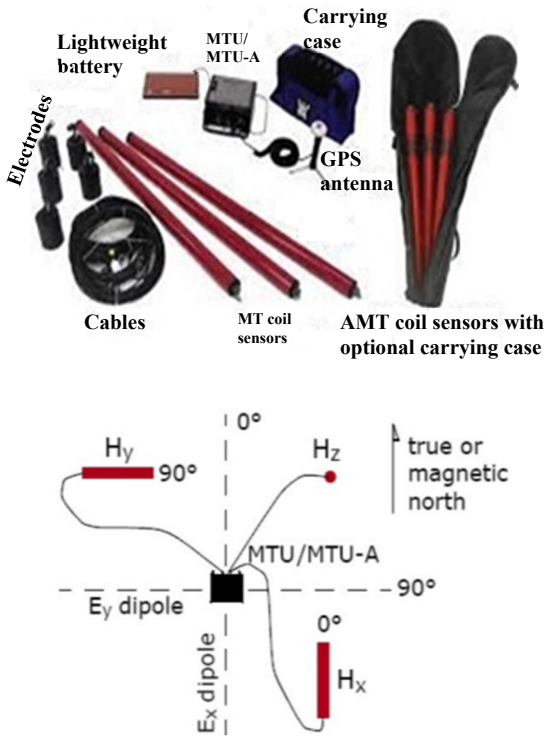

FIGURE 17: MT data acquisition system and field layout (Phoenix Geophysics, 2009)

Five sets of MT equipment of Phoenix type (MTU's) were used. MTC50H and MTC80H induction coils measured the horizontal and vertical components, respectively, as shown in Figure 17. One MT system was used for remote reference at a site located in Corbetti area some 80 km NE of the survey area. The site is called ABA000 in Appendix 1 (REF). This is a standard method to get better quality result in data processing. The other four instruments were deployed every day and picked up the next day. However, soundings where often left for more than a day, both because of insufficient time during the day to move it and sometimes the instruments were restarted for another night due to insufficient data quality. Before a site was picked up, a portion of the time series was preliminary analysed in the field for data quality control. Based on the outcome, the site was either picked up or started again after some adjustments. The data are sampled at three sampling frequencies, i.e., at 2400 Hz, 150 Hz and 15 Hz. The first two bands are sampled at every other minute for 2 and 16 seconds, respectively, while the third band is sampled continuously. This gives MT data from 320 Hz (0.003 sec) to over 1000 seconds.

There were 13 MT soundings used for joint inversion while 4 soundings were not used due to bad data quality. The listing of all the MT sites with their locations is found in Appendix 1 (REF).

The measured MT time series data are Fourier transformed into the frequency domain and the "best" solution is found that describes the relation between the electrical and magnetic fields as described in equation 18.

The raw data in TBL format are used to process the time-series signal by a program from Phoenix Ltd, SSMT2000, commonly using a robust processing technique (Figure 18). The result was edited in the MTEditor program by Phoenix (Figure 19).

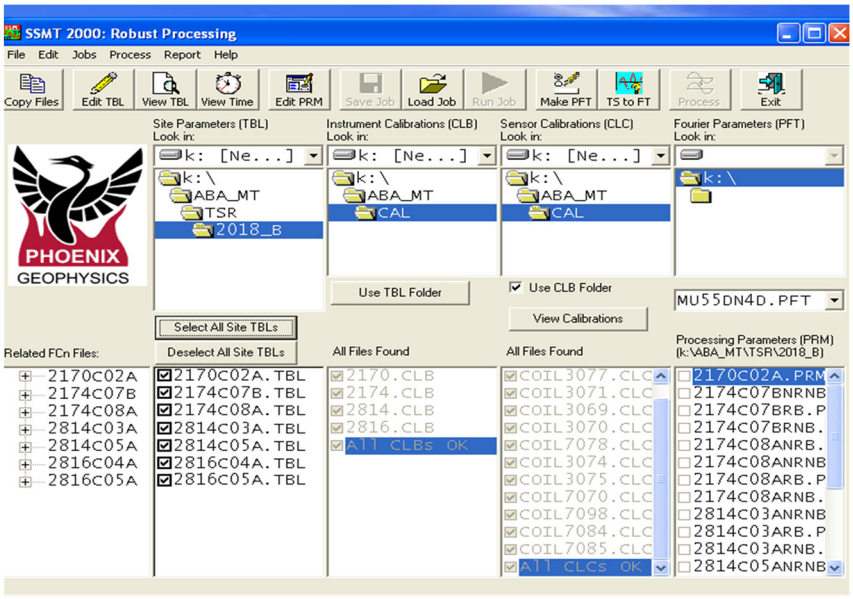

FIGURE 18: SSMT2000 processing software

The processed MT data in terms of magnitude (apparent resistivity) and phases of measured impedance elements are given in Appendix 3 (REF). From this result, other MT parameters like coherency, principal direction, 2D and 3D indicators and Tipper information (relation between components of the magnetic field) were calculated using a program called spect2edi and the results set in a standard EDI file format. These results are plotted in Figure 20 and are given in Appendix 3 (REF).

From the impedances the apparent resistivity and phase are calculated at different periods, T according to:

$$\rho_{xy} = 0.2T\,|Z_{xy}|^2 \; ; \; \theta_{xy} = \arg(Z_{xy})$$

$$\rho_{yx} = 0.2T\,|Z_{yx}|^2 \; ; \; \theta_{yx} = \arg(Z_{yx})$$

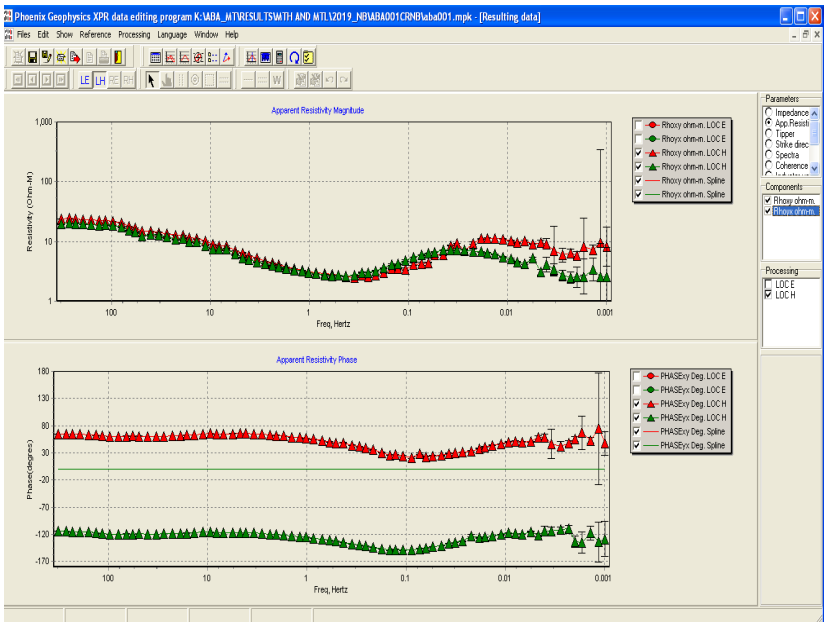

FIGURE 19: Editing data from sounding ABA001 with MTEditor

The results from the Abaya data show that the diagonal elements of the impedance tensor (Z_{xx} , Z_{yy}) are usually 2 to 4 orders of magnitude smaller than the off-diagonal elements (Z_{xy} *and* Z_{yx}). We, therefore, generally have $\rho_{xy} \sim \rho_{yx}$. This shows that the data are mostly one dimensional in nature. Only at periods greater than 10 seconds ρ_{xy} and ρ_{yx} become slightly different.

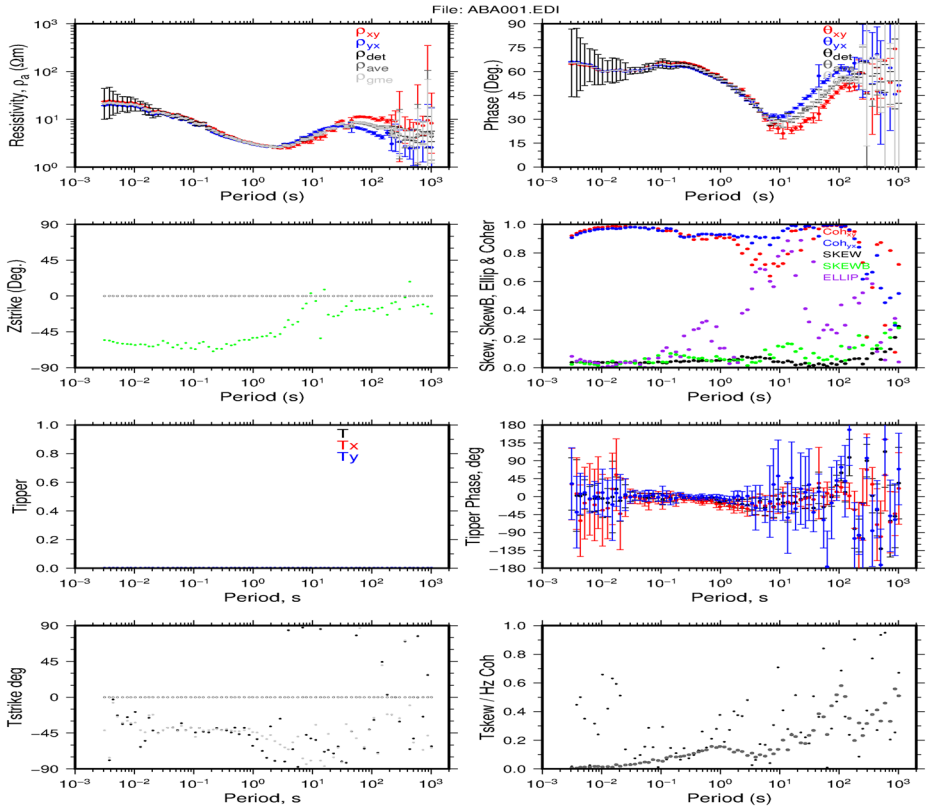

FIGURE 20: Plot of EDI file from sounding ABA001

Figure 20 shows MT data from site ABA001 located near to Abaya Lake and close to geothermal surface manifestations along the Abaya fault (Figure 14). The top frame shows the apparent resistivity and phase, both plotted as a function of the period which is kind of a depth scale. The two modes ρ_{xy} *and* ρ_{yx} are very similar, both for the apparent resistivity and phase. This indicates a mostly 1D resistivity structure with depth. The resistivity ρ_{xy} *and* ρ_{yx} plots at ABA051 site shown in Figure 21 reveal a resistivity structure that is roughly 1D in nature up to few seconds, but at longer periods strong 2D structure is observed. This demonstrates how the resistivity curves vary with period and how the subsurface resistivity dimensionality does affect the data. The small shift in the apparent resistivity curves at low periods (high frequency) is due to "static shift" caused by resistivity inhomogeneity near the surface. The two curves exhibit the same character for high frequencies down to 1 Hz. Thus, we can expect that a 1D interpretation of the data is accurate down to depths somewhat below the clay cap layer. Generally, the MT data quality at long periods is worse than expected from comparison to other MT surveys in Ethiopia that RG has conducted. One reason could be the high resistive ground resulting in high contact resistance of the electrodes. The signal strength is also weaker than in previous surveys due to the 11 years periodicity of the sunspot activity and at the time of data acquisition the activity was at its minimum. Those sunspots are the source of the long period MT signal.

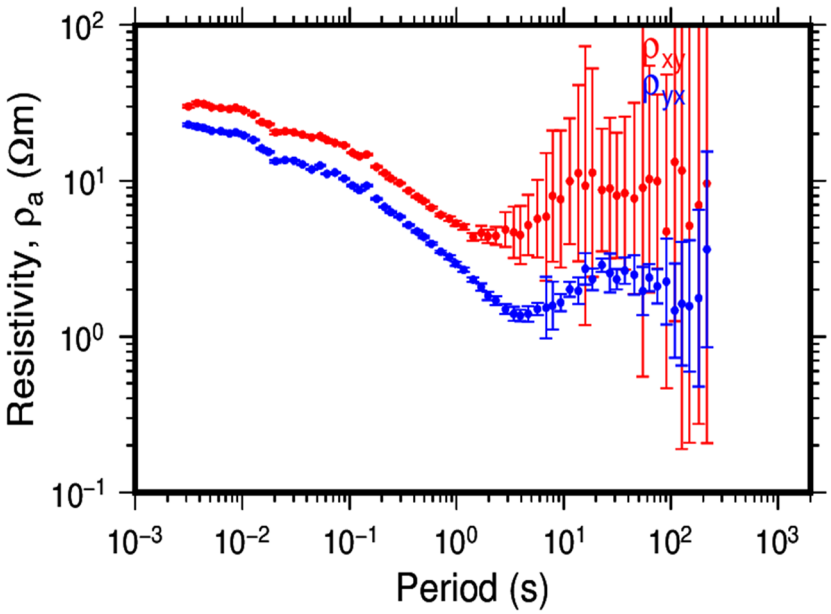

FIGURE 21: ρ_{xy} *and* ρ_{yx} plots at ABA051 site that shows static shift and different dimensionalities with

5. DATA INVERSION

Each MT/TEM sounding pair is inverted jointly such that the same 1D resistivity model explains both data sets. 1D means that the resistivity of the Earth only varies with depth, and the inversion is done by a program where the model parameters are determined such that the calculated response of the 1D model fits the measured data. The inversion algorithm applied (Occam inversion) finds the simplest 1D model whose response fits the data. These 1D models from each site are then compiled into a visual pseudo-3D resistivity model by interpolation. The end results are horizontal and vertical resistivity sections through the final model.

An example of an inversion for site ABA001 is shown in Figure 22. We observe high-low-high-low resistivity structures with depth. The first low resistivity layer is possibly the clay cap, and the second low resistivity layer is a deep conductor interpreted as the heat source (possibly magma) for the geothermal system.

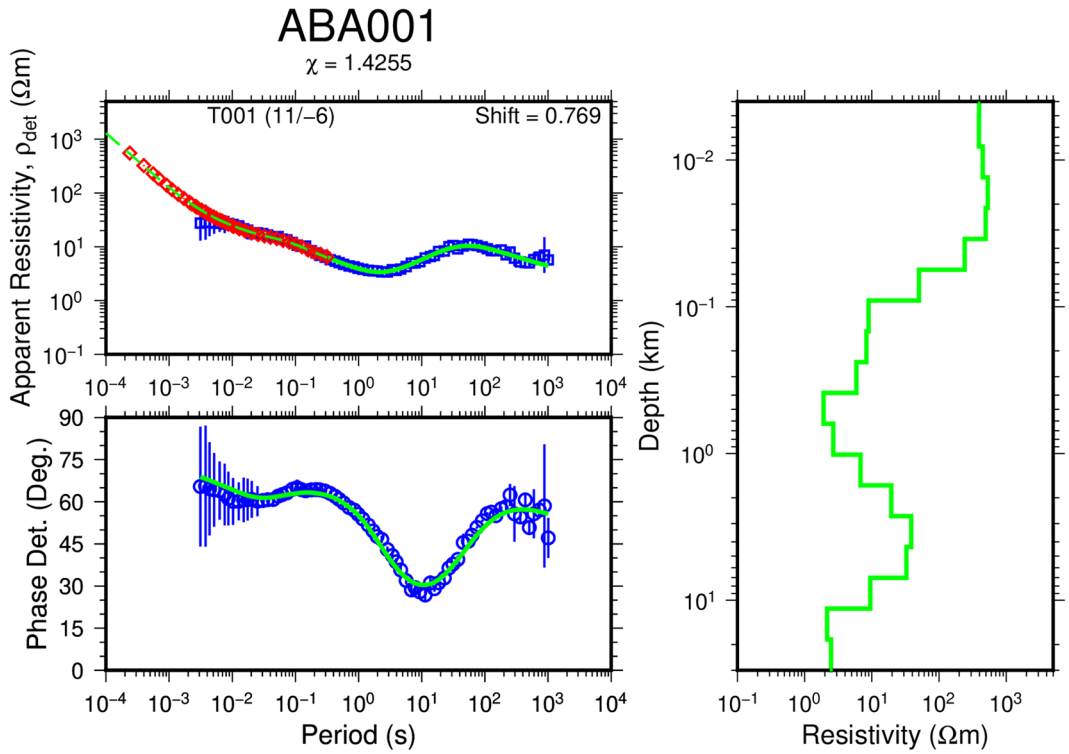

FIGURE 22: Example of joint inversion result of ABA001 and T001. Upper left-hand side: Determinant apparent resistivity vs. period. Red squares are TEM soundings, and the blue ones are MT soundings. The green line is the model response of the joint inversion. Lower left-hand side: Phase of the determinant vs. period. The blue circles are the phase, and the green line is the predicted phase from the model. On the right: best model for the joint inversion of MT and TEM data for sounding ABA001

5.1 Determinant-apparent resistivity and phase

In a 1D inversion it is not clear which of the MT parameters should be used, whether one should use the xy or yx parts of the impedance and what rotation should be used. Alternatively, one could use a combination of these two modes, and preferably parameters which are not dependent on horizontal rotation (i.e., rotationally invariant) and in some sense represent the "best" 1D effects in the data. Three such data representations have been proposed, that is:

$$Z_{ave} = \frac{Z_{xy} - Z_{yx}}{2}$$
$$Z_{det} = \sqrt{Z_{xx}Z_{yy} - Z_{xy}Z_{yx}}$$
$$Z_{gme} = \sqrt{-Z_{xy}Z_{yx}}$$

When the Earth is purely 1D, all these parameters give the same values. For a 2D Earth, the det (determinant) and the gme (geometric mean) reduce to the same value but the ave (arithmetic mean or effective) is different. For a 3D Earth, all those parameters differ.

It is not clear which of the three invariants is best suited for 1D inversion. Several scientists have suggested that the determinant invariant is the one to use based on comparison of model responses for 2D and 3D models (Park and Livelybrook, 1989; Rangabayaki, 1984; Ingham, 1988), and hence, it has been chosen here for the 1D inversion were possible.

5.2 1D inversion procedure and telluric shift

The inversion program used here is called TEMTD and was developed by Iceland GeoSurvey (Árnason, 2006). One option is to use the Occam inversion procedure which minimizes the model structure and generates smooth models (Constable et al., 1987; deGroot-Hedlin and Constable, 1990). This means that out of the infinitive number of models whose response fits the data, the Occam inversion algorithm seeks models that have the smallest resistivity structure and are smooth. The program inverts jointly for both TEM and MT data and it can also find the "best" *static shift* (see below) parameter for the MT data. Thus, it generates a 1D resistivity model whose response fits both the MT and TEM data and at the same time determines the static shift for the MT data.

The static shift of MT data in the Abaya prospect area could be caused by near-surface resistivity structures close to the site, current channelling, and/or topography. It only affects the electric field but causes the apparent resistivity to be shifted (by a multiplier) and can thus leads to a false interpretation. A histogram of all the telluric shifts from the MT sites is shown in Figure 23 on a linear scale. The static shift multiplier used for MT data range from 0.5 to 1 but the average shift multiplier is 0.7 on a linear scale. A linear shift value of 0.7 means that the measured apparent resistivity has been shifted down by an order of magnitude due to local resistivity inhomogeneity, thus the measured apparent resistivity data must be divided by 0.7 to get the correct value.

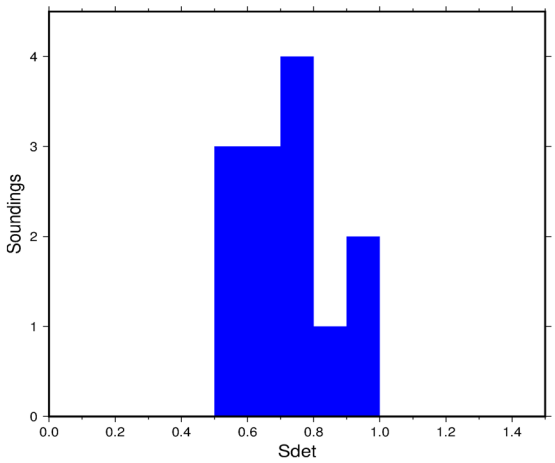

FIGURE 23: Histogram of resistivity static shift values for all the Abaya MT sites

The TEM site is set up at the same location, or close to that of the MT site. Table 1 in Appendix 1 (REF) shows the TEM sounding used for the static shift correction of each MT sounding as well as the shift factor for each sounding. The inversion results of all the MT soundings are given in Appendix 4 (REF). Figure 24 shows both inversion results of the original MT data (un-shifted) (black coloured model) as well as the joint inversion result of the TEM and the MT data (green coloured model). The shift result for the joint inversion is 0.573, i.e., the original data had to be divided by that value in order to fit both MT and TEM data by the same model. This is an upward shift of about 1/4 of a decade ($\log_{10}(0.573) = 0.24$). As expected, the inversion result of the un-shifted data gives a model with lower resistivity values and depths are shifted upwards compared to the inversion result of the shifted data. The phase is the same for both shifted and un-shifted data.

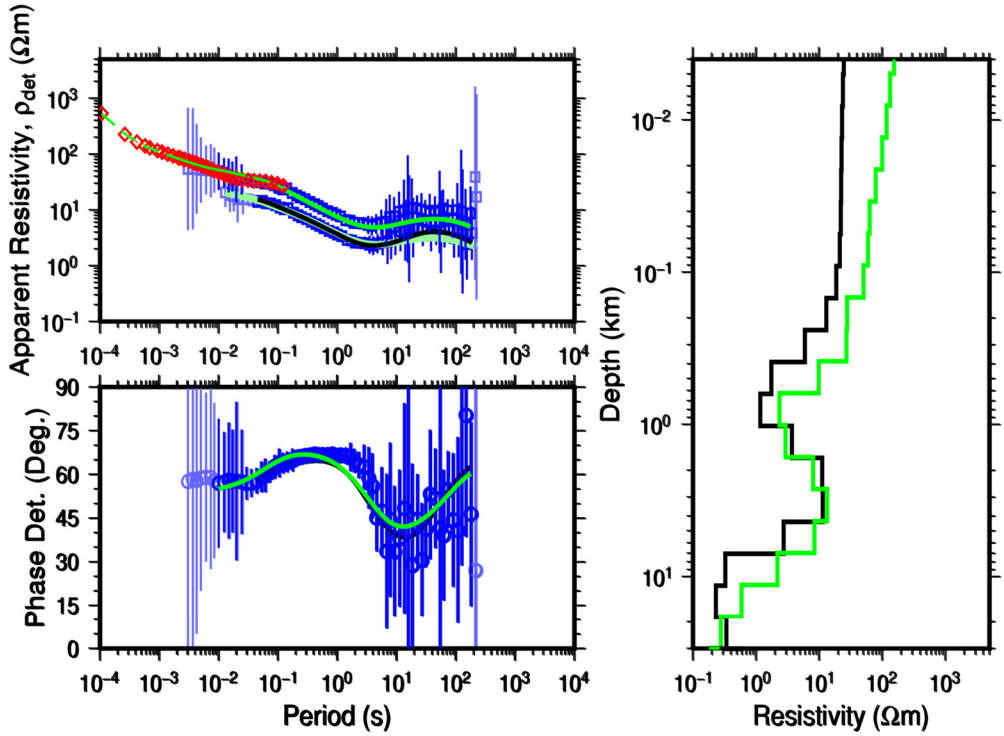

FIGURE 24: Inversion of MT sounding ABA056, without static shift and by using a joint inversion of MT and TEM data with static shift correction. Green and black models and response curves are with and without static shift, respectively

5.3 Strike analysis

Tstrike and Zstrike

Examples of T-strike and Zstrike analysis in the Abaya geothermal project area for periods ranging from 1 to 10 s are shown in Figures 25 and 26, respectively. The geoelectrical strike is a direction representing the orientation of electric current flow in the subsurface due to lateral inhomogeneity of electric conductivity in the Earth (Niasari, 2016). The low periods provide information on strike direction at shallow depth. The rose diagrams of the T-strikes and Zstrikes are mostly oriented in EW and SE to NW direction, which is nearly perpendicular to the general direction of the geological structures or faults in the Main Ethiopian Rift. The result of the strike analysis supports that there is an elongated electrical boundary along easterly dipping direction of Abaya fault which could be acting as a conduit for fluid movement.

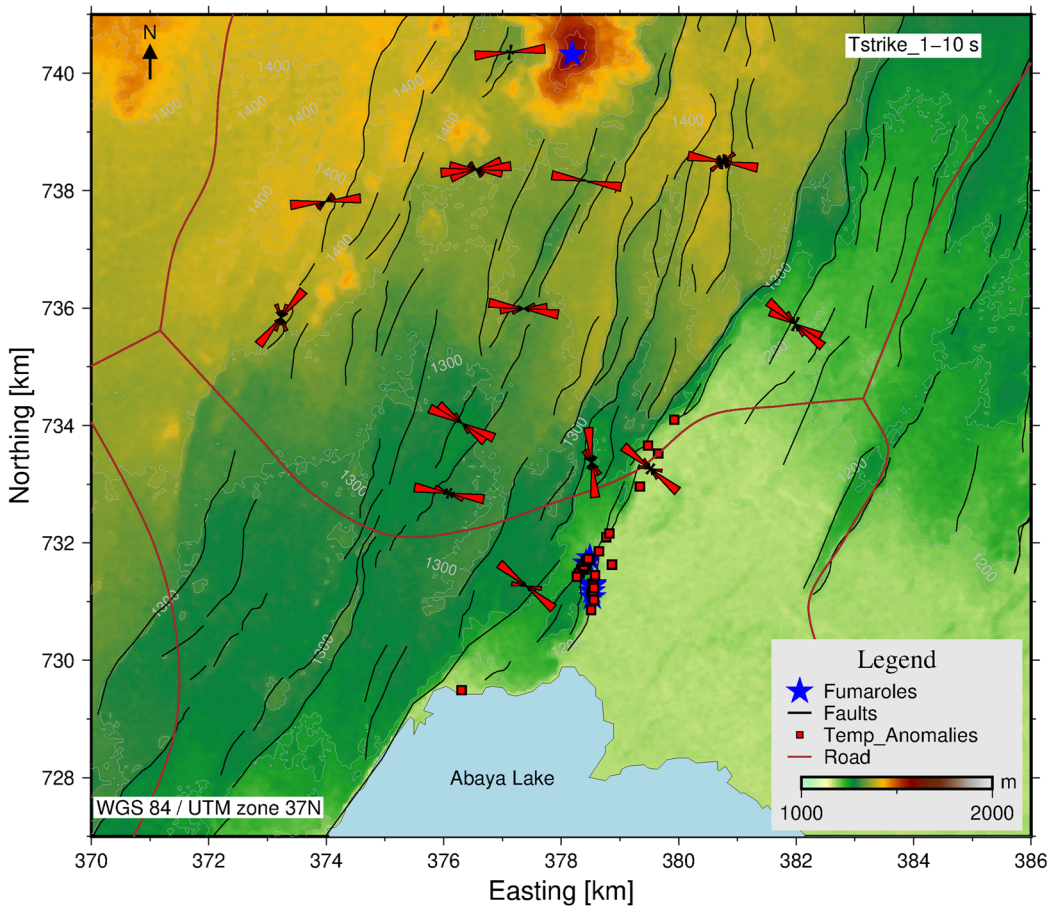

FIGURE 25: Tipper strike for the period range between 1- 10 s in Abaya prospect area in southern Ethiopia

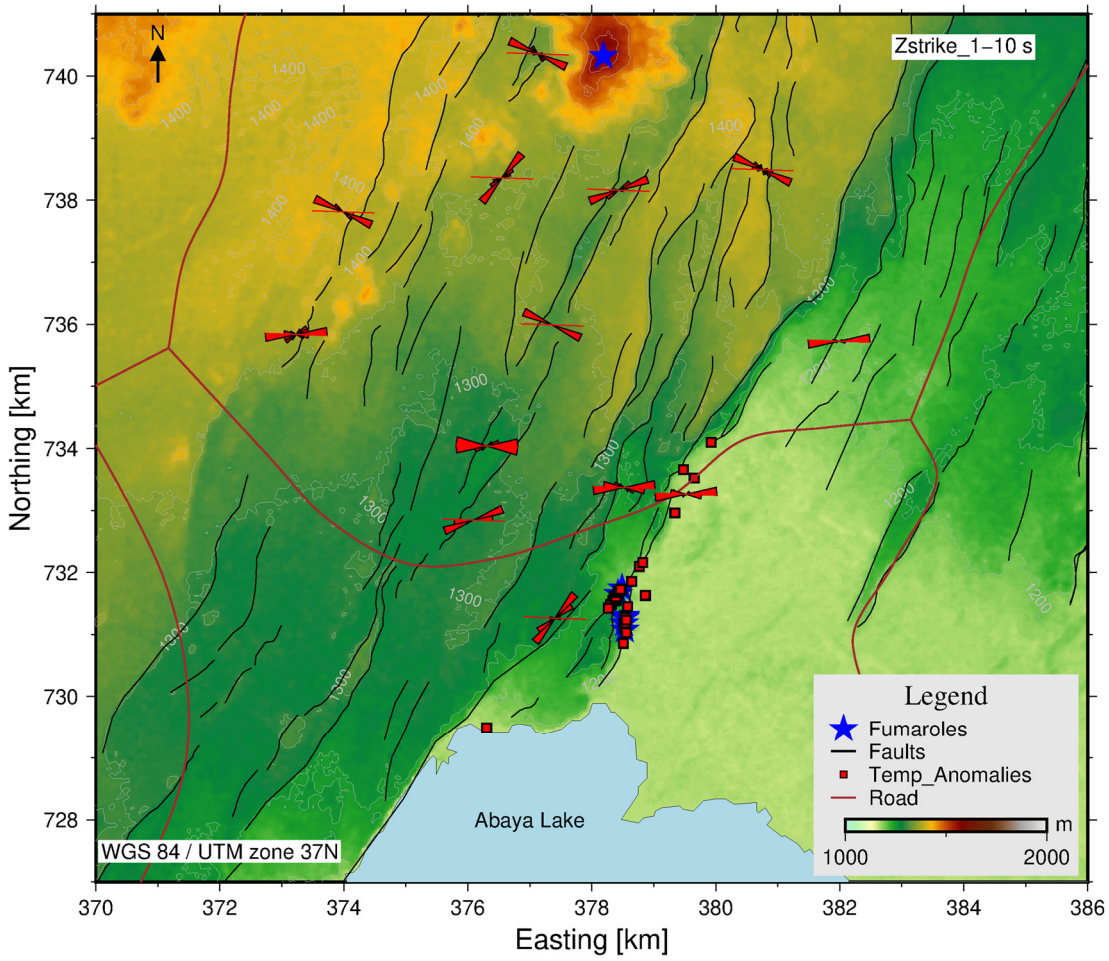

FIGURE 26: Zstrike for the period range 1- 10 s in Abaya prospect area in southern Ethiopia

Induction arrow

The complex ratio of horizontal and vertical components of magnetic fields is represented by induction arrows (Naidu, 2011). They give information about lateral variations in conductivity (Jupp and Vozoff, 1976). Insulator/conductor boundaries extending through a 2-D Earth give rise to induction arrows that orient perpendicular to them, and their magnitude indicates the intensities of anomaly current concentrations (Wiese, 1962). The real part of the vector points towards the anomalous internal concentrations of current (Simpson and Bahr, 2005) called Parkinson convention while it points away from the internal current concentrations called Wiese convention.

Figure 27 shows induction arrows at 5 s in the Abaya prospect area, southern Ethiopia, according to Wiese convention. The size and distribution of the induction arrows are not uniform and the direction of most of the real vectors (in blue) in the northern part of the project area is north what indicates the presence of low resistivity zone in opposite direction.

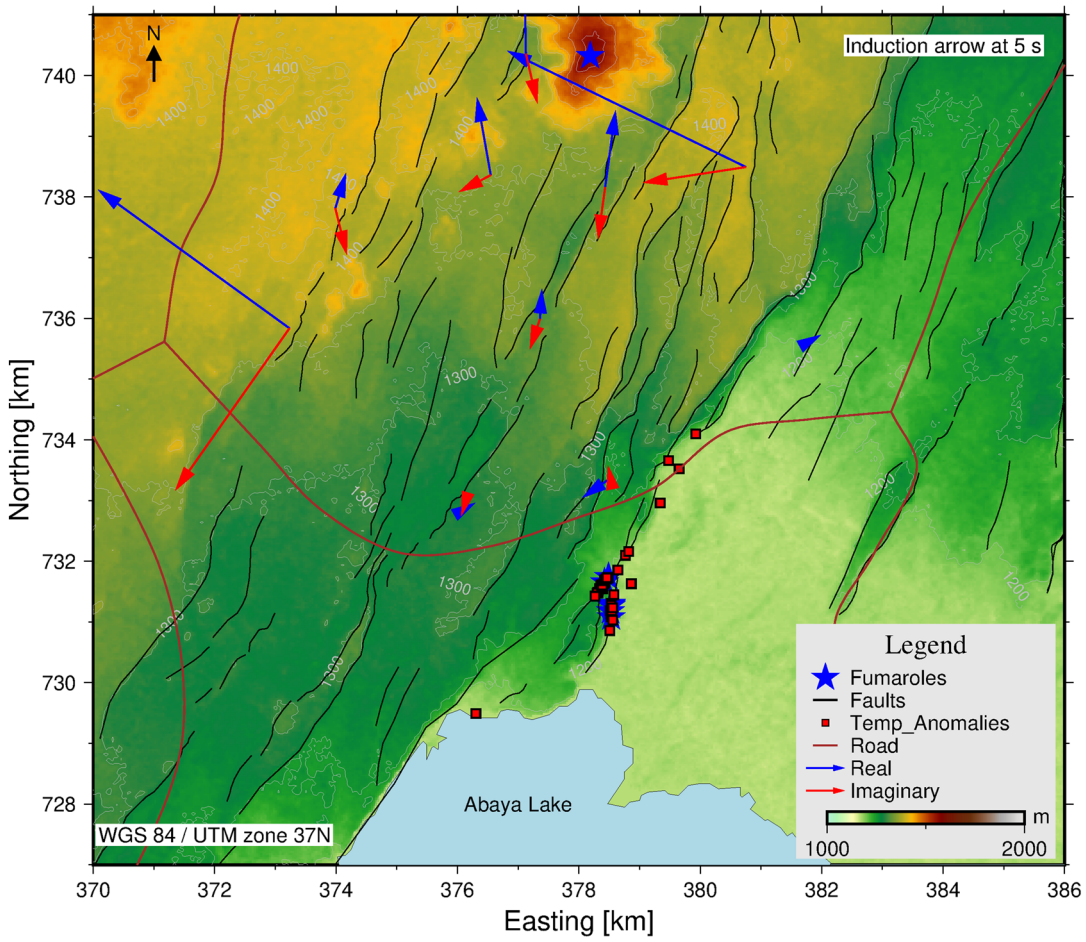

FIGURE 27: Induction arrows at 5 s from Abaya prospect area in southern Ethiopia, according to Wiese convention.

6. RESULTS

The result of the joint inversion of the MT/TEM soundings are interpreted here and presented as horizontal resistivity maps at different depth and as resistivity cross-sections. Figure 15 shows the location of the two resistivity cross-sections discussed below. All cross-sections and horizontal maps are found in Appendix 4 (REF).

6.1 Cross-sections

6.1.1 The resistivity cross-section along PL_06

The resistivity of the SW-NE trending cross-section along PL_06 is presented in Figure 28 down to two different depths. This section is produced using three soundings: ABA001, ABA078 and ABA082. The distance between the soundings is not uniform and the total length of the profile is about 9 km. The resistivity cross-section on the left side of Figure 28 shows the resistivity structure down to sea level and the resistivity cross-section on the right side shows the model down to 5 km below sea level. The resistivity cross-section shows the main result of the resistivity survey. A low resistivity layer (< 10

Ωm) at shallow depth is roughly 1500 m thick and is clearly seen in the section down to 5 km below sea level. This layer can be interpreted either as the clay cap of the geothermal system or a saline sedimentary layer. The intermediate-resistivity zone under sounding ABA082 on the cross-section down to 5 km below sea level could be caused by high temperature clay minerals such as epidote and chlorite. The reason why it is not under all the conductive layer could be because of Abaya fault.

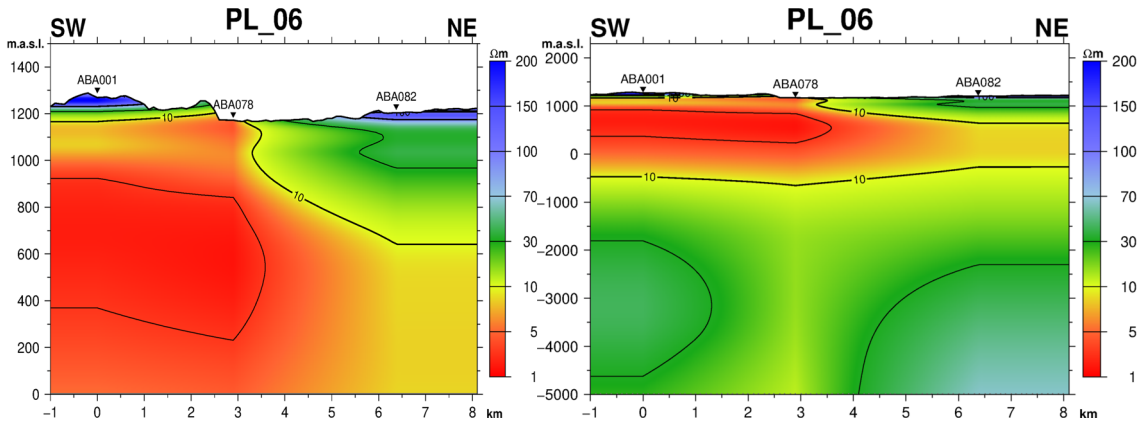

FIGURE 28: Resistivity cross section along PL_06 down to sea level and 5 km depth. Location of the cross section is given in Figure 15. See text for details

6.1.2 The resistivity cross-section along PL_05

Figure 29 shows a WNW to ESE lying resistivity cross-section along PL_05. It indicates a similar resistivity structure as seen in cross-section PL_06. A deep conductor is visible in the soundings composing section PL_05. The depth to the deep conductor is quite irregular as shown on the cross-section down to 10 km (see Appendix 4 (REF)) which is not surprising since the data are not 1D for most of the soundings at long periods. The resolution of the resistivity model at this depth is, however, quite limited. On both cross-sections along PL_06 and PL_05, the existence of a fault dipping to the east is evident. This fault could be correlated to the Abaya fault which is oriented in NE-SW direction (Figure 14). The resistivity survey at the Abaya project strongly supports the findings from the analysis of the geology, the surface manifestations, the temperature, and the gas flux results of the area. Other cross-sections shown in the Appendix 4 (REF) and the resistivity maps shown below confirm those findings.

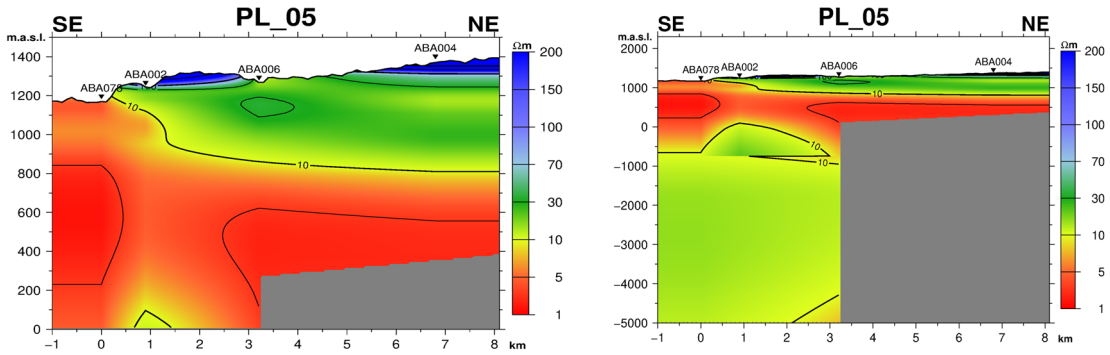

FIGURE 29: Resistivity cross section along PL_05 down to sea level and 5 km depth. Location of the cross section is given in Figure 15

6.2 Horizontal resistivity maps

Examples of horizontal resistivity maps at 800 m a.s.l., 400 m a.s.l, 0 m and at 1800 m b.s.l are shown in Figure 30. The low-resistivity layer covers almost the whole area of the horizontal resistivity map at 400 m a.s.l. However, the thickness of this layer decreases towards the southeast part of the project area. The values of the low resistivity layer are generally ranging from 2 up to 10 Ωm. The high resistivity zone is clearly outlined north of Lake Abaya towards the NE along the Abaya fault where surface manifestations are located (Figure 15).

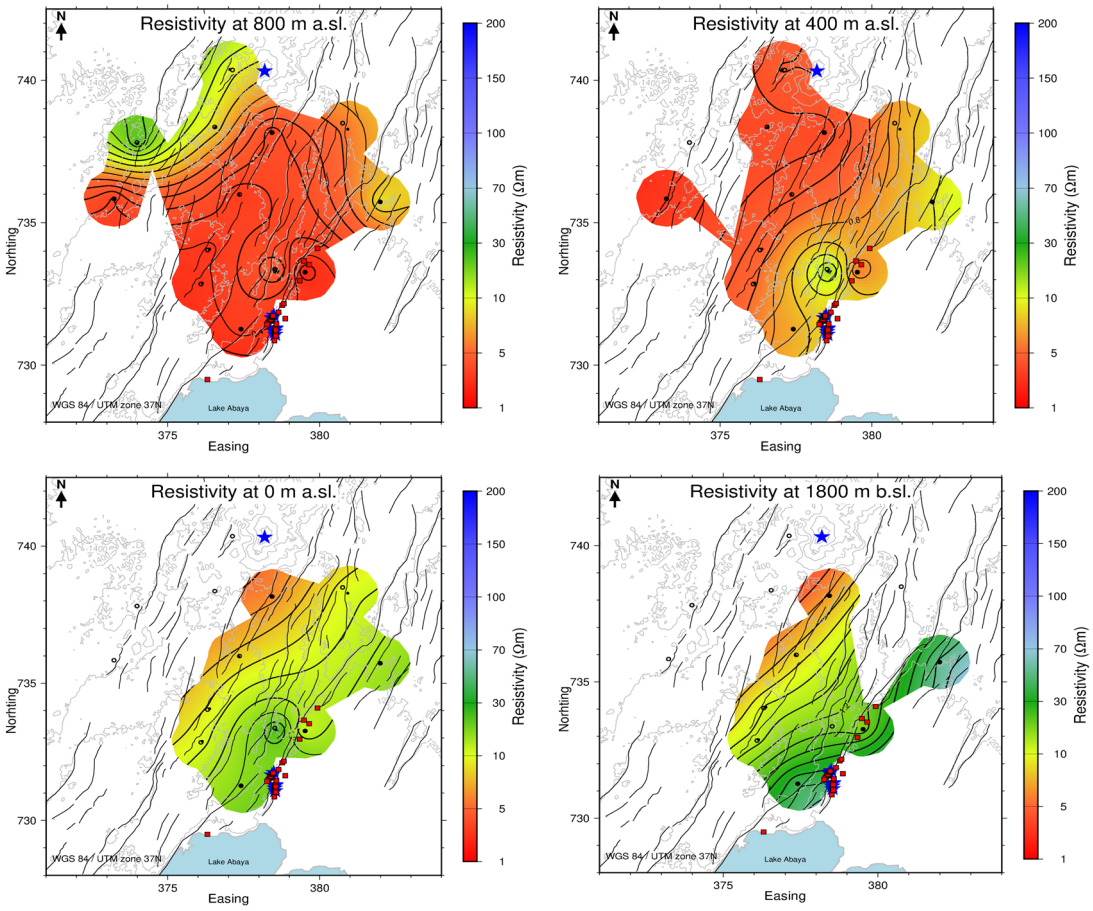

FIGURE 30: Horizontal resistivity maps
at 800 m a.s.l, 400 m a.s.l, sea-level, and at 1800 m b.s.l. For figure legend, see Figure 15

7. CONCLUSION

Main resistivity characteristics

The resistivity structure of the Abaya geothermal area is consistent with what can be expected in high enthalpy geothermal systems. The main features can be summarized by the following:

- High resistivity close to the surface;
- A low resistivity layer is mapped at shallow level. This layer could be interpreted either as the clay cap overlaying a geothermal reservoir or a saline sedimentary layer;
- The average thickness of the shallow low-resistivity layer is around 1.5 km and its resistivity is generally 2-10 Ωm, higher towards the north;
- Below this layer the resistivity is generally 50-100 Ωm; and
- A second conductor is mapped in the upper crust at roughly 9 km depth – however, the resolution of the model at this depth is rather poor.

The existence of a shallow low-resistivity layer may be due to temperature dependent alteration of minerals. This process is dependent on rock and water chemistry as well as temperature. In basaltic rocks, zeolites and

smectite are formed in the temperature range of 80-230°C, while from 230-250°C the smectite is transformed into chlorite. Epidote is formed at temperatures exceeding 250°C (Kristmannsdóttir, 1979). Smectite is a low-temperature clay mineral. Its presence has been observed in many high-enthalpy geothermal reservoirs worldwide. It forms a conductive clay cap on top of the geothermal systems underlain by a resistive chlorite/epidote zone. (Árnason et al., 2000; Johnston et al.; 1992; Eysteinsson et al., 1994, 2013, 2015; Cumming and Mackie, 2010, Eysteinsson, 2015, 2017, Samrock et al., 2015, 2018; Hersir et al., 2022).

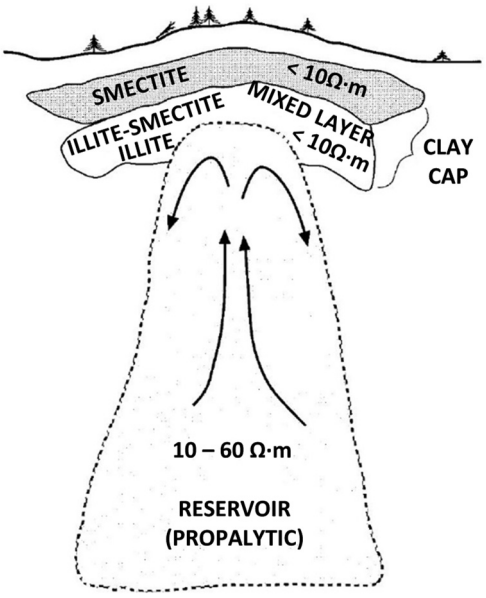

FIGURE 31: A generalized picture of a geothermal system. The well conducting clay-cap layer is on the top of the reservoir system (Pellerin et al., 1996)

The shallow low resistivity layer

We cannot determine if the shallow low-resistivity layer is formed by conductive alteration minerals or saline sediments or a combination of both.

If the low-resistivity layer is a clay-cap, one can expect a temperature of 200-250°C, provided the thermal alteration is in thermal equilibrium with reservoir temperature at present. It takes time for the chemical reactions between the water and the rock (alteration) to take place, hence, young geothermal systems may experience higher temperature than is indicated by the thermal alteration. We may also see the opposite, where the geothermal system has cooled down, but the alteration still prevails. Hence, the thermal alteration will only represent the true temperature if it is in thermal equilibrium and could only represent the maximum temperature that a geothermal system has been subjected to in the past.

The permeability will also affect the degree of alteration. Without permeability there is no water to alter the rock, even at high temperatures. This means that if the large-scale permeability is variable throughout the geothermal system it will be reflected in the resistivity as well.

The resistivity models used here are “continuous” and therefore it is not straight forward to determine the depth range of the low-resistivity layer. One way to do this in a systematic manner is to define the low-resistivity layer by a maximum resistivity value, for example 10 Ωm, as is done in Figure 32. The red vertical line on the model shows the 10 Ωm line and the clay cap layer would be in the depth interval between the top two horizontal brown lines. This gives the thickness of the low-resistivity layer at this site which is around 1.5 kilometres.

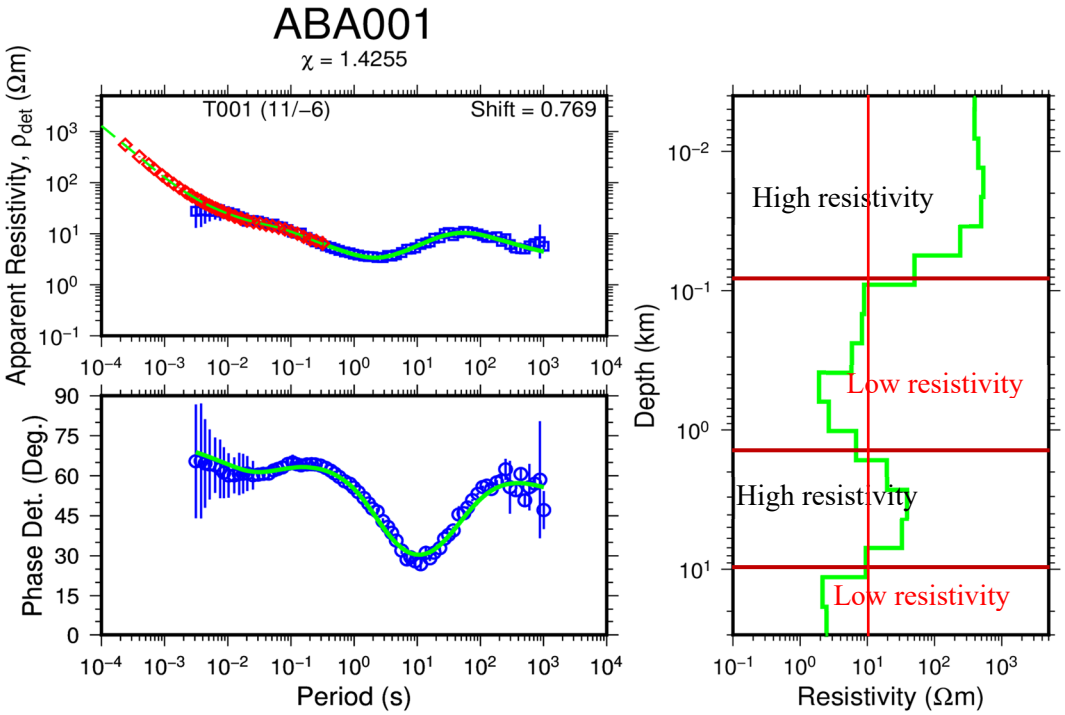

FIGURE 32: Inversion of TEM/MT sounding ABA001. The top low resistivity (100 meter – 1.5 km below sea level) and the bottom (10 km below sea level) low resistivity layers are determined where the resistivity is lower than 10 Ωm

The deep conductor

The depth to the top of the deep conductive layer at about 10 km below sea level and it could represent the heat source of the geothermal system in Abaya.

A deep conductor such as found here, is frequently seen in other high enthalpy geothermal systems around the world at similar depths (e.g., Iceland, Kenya, Mexico). In the Main Ethiopian rift zone (MER) such a layer is found in the Corbetti geothermal area located some 80 km NE of Abaya (Gíslason et al., 2012; Eysteinsson, 2013), and at Tulu Moye 215 km NNE from Abaya (Eysteinsson et al., 2015; Eysteinsson, 2017), but is not observed in the recent MT survey in Aluto-Langano geothermal field nor in the MER some 160 km to NE of Abaya (Samrok et al., 2015). A similar deep conductor was also found in an MT survey by Whaler and Hautot (2006) crossing the MER at around 8.5°N latitude, some 260 km NE of the Abaya, at about 15 km depth. Such a deep conductor is also found in the Tendaho region some 650 km NNE of Abaya in the Afar region (Lemma Didana et al., 2014).

ACKNOWLEDGEMENTS

First and foremost, I would like to praise and thank God, the Almighty, who has granted me peace and health so that I have finally been able to accomplish my project work.

I would like to express my special gratitude to the entire GRÓ GTP staff, Director of GRÓ GTP Mr. Guðni Axelsson, Deputy Director Mr. Ingimar G. Haraldsson, Ms. Málfrídur Ómarsdóttir, Ms. Vigdís Harðardóttir and Mr. Markús A.G for allowing me to attend the six-month geothermal training program.

I would like to express my sincere gratitude to my supervisors Ásdís Benediktsdóttir, Gylfi Páll Hersir and Knútur Árnason for their continuous follow-up, guidance and support.

I would like to thank all GTP fellows for the good time we spend together and the experiences we shared. I wish to thank Iceland GeoSurvey (ÍSOR) for providing access to facilities and training required for successful completion of the six-month geothermal training.

I would like also to thank Reykjavik Geothermal and in particular Hjálmar Eysteinsson geophysicist for permission to use their MT and TEM data and display some of the results of their studies on the Abaya prospect area.

My deepest appreciation goes to my wife Feven and my daughters Yohanna and Eldana for their unconditional love and support throughout my entire six-month geothermal training.

REFERENCE

Archie, G.E., 1942: The electrical resistivity log as an aid in determining some reservoir characteristics. *Tran. AIME, 146,* 54-67.

Árnason, K., 1989: *Central loop transient electromagnetic sounding over a horizontally layered earth*. Orkustofnun, Reykjavík, report OS-89032/JHD-06, 129 pp.

Árnason, K., Haraldsson, G.I., Johnsen, G.V., Thorbergsson, G., Hersir, G.P., Saemundsson, K., Georgsson, L.S., Rögnvaldsson, S.Th., and Snorrason, S.P., 1987: Nesjavellir-Ölkelduháls. Surface exploration in 1986. Orkustofnun, Reykjavík, report OS-87018/JHD-02 (in Icelandic), 112 pp + maps.

Árnason, K., Karlsdóttir, R., Eysteinsson, H., Flóvenz, Ó.G., and Gudlaugsson, S.Th., 2000: The resistivity structure of high-temperature geothermal systems in Iceland. *Proceedings of the World Geothermal Congress 2000*, *Kyushu-Tohoku, Japan,* 923-928.

Árnason, K., 2006: *TEMTD, a program for 1D inversion of central-loop TEM and MT data. Short manual*. ÍSOR – Iceland GeoSurvey, Reykjavík, Iceland, internal report, 17 pp.

Árnason, K., Eysteinsson, H., Hersir, G.P., 2010: Joint 1D inversion of TEM and MT data and 3D inversion of MT data in the Hengill area, SW Iceland. *Geothermics*, *vol 39*, 13-34.

Bendick, R., Bilham, R., Asfaw, L., and Klemperer, S., 2006: Distributed Nubia-Somalia relative motion and dyke intrusion in the main Ethiopian rift. *Geophysical J. International, 165,* 303–310.

Chernet, Tadiwos., 2011: Geology and Hydrothermal Resources in the Northern Lake Abaya Area (Ethiopia). *Journal of African Earth Sciences,* 61(2), 129–41.

Constable, S.C., Parker, R.L., Constable, C.G., 1987: Occam´s inversion: A practical algorithm for generating smooth models from electromagnetic sounding data. *Geophysics, 52-3,* 289-300.

Corti, G., 2009: Continental rift evolution: From rift initiation to incipient break-up in the Main Ethiopian Rift, East Africa. *Earth-Science Reviews*, 96, 1–53.

Corti, G., Philippon, M., Sani, F., Keir, D., and Kidane, T., 2013: Re-orientation of the extension direction and pure extensional faulting at oblique rift margins: Comparison between the Main Ethiopian Rift and laboratory experiments. *Terra Nova, 25,* 396–404.

Cumming, W., and Mackie, R. 2010: Resistivity Imaging of Geothermal Resources Using 1D, 2D and 3D MT Inversion and TDEM Static Shift Correction Illustrated by a Glass Mountain Case History. *Proceedings of the World Geothermal Congress 2010 Bali, Indonesia*, 25-29

Dakhnov, V.N., 1962: Geophysical well logging. *Q. Colorado Sch. Mines, 57*, no. 2,445 pp.

deGroot-Hedlin, C., Constable, S., 1990: Occam inversion to generate smooth, two dimensional models from magnetotelluric data. *Geophysics*, 55, 1613-1624.

Dobrin, M.B., and Savit, C.H., 1988: *Introduction to geophysical prospecting*. McGraw-Hill publ., NY, 867 pp.

Domra Kana, J. Djongyang, N., Danwe, R., Njandjock Nouck, P., Abdouramani, D., 2015: A review of geophysical methods for geothermal exploration. *Renewable and Sustainable Energy Reviews, 44*, 87-95. Available at: *https://www.sciencedirect.com/journal/renewable-and-sustainable-energy-reviews/vol/44/suppl/C*

Ebinger, C., 2005: Continental break-up: The East African perspective. *Astronomy and Geophysics, 46,*16–21.

Eysteinsson, H., Árnason, K., Flóvenz, Ó.G., 1993: Resistivity methods in geothermal prospecting in Iceland. *Surveys in Geophysics, 15,* 263-275.

Eysteinsson, H., 2013: *Resistivity at Corbetti Geothermal prospect. Part II.* Reykjavik Geothermal internal report No:100028-05B, 21 pp and 7 appendices.

Eysteinsson, H., Gíslason, G., and Guðmarsson, T., 2013: *Assessing the Ceboruco geothermal potential by resistivity mapping and cross correlation with other data.* Reykjavik Geothermal report No:100043-01, 56 pp and 7 appendices.

Eysteinsson, H., 2015: *Resistivity study of Mt. Soufriere, Saint Vincent and the Grenadines.* Reykjavik Geothermal internal report No:13002-03, 40 pp and 7 appendices.

Eysteinsson, H., Jónsson, S.B., and Tekka, A.H., 2015: *Resistivity study of the Tulu Moye Geothermal Prospect, Ethiopia. Part II. Resistivity exploration.* Reykjavik Geothermal internal report No. 13001-02, 51 pp and 7 appendices.

Eysteinsson, H., 2017: *Resistivity study of the Tulu Moye Geothermal Prospect, Ethiopia. Resistivity exploration.* Reykjavik Geothermal internal report No. 17006-07, 22 pp and 7 appendices.

Flóvenz, Ó.G., Georgsson, L.S., and Árnason, K., 1985: Resistivity structure of the upper crust in Iceland, *J. Geophys. Res., 90-B12,* 10,136-10,150.

Flóvenz, Ó.G., Spangerberg, E., Kulenkampff, J., Árnason, K., Karlsdóttir, R., Huenges, E., 2005: The role of electrical interface conduction in geothermal exploration. *Proceeding of the World Geothermal Congress 2005, Antalya, Turkey,* 9 pp.

Flóvenz, Ó.G., Hersir, G.P., Saemundsson, K., Ármannsson, H., and Fridriksson, Th., 2012: Geothermal energy exploration techniques. In: Sayigh, A. (ed.), *Comprehensive Renewable Energy, 7.* Elsevier, Oxford, UK, 51-95.

Gebregziabher, Z., 1997: Ethiopian geothermal resources and their characteristics, *Geothermal Resource council Transactions, Vol 21, Ethiopian Institute of Geological Surveys*.

Georgsson, L.S., 2013: Geophysical methods used in Geothermal exploration. *Proceedings of Short Course VIII on Exploration for Geothermal Resources, organized by UNU-GTP, GDC and KenGen, Lake Bogoria and Lake Naivasha, Kenya,* 16 pp.

Gíslason, G., Eysteinsson, H., Hardardóttir, V., and Björnsson, G., 2012: *Corbetti Geothermal Prospect. Surface Exploration: Geology, geochemistry and resistivity report. Report to the Federal Democratic Republic of Ethiopia, Ministry of mines.* Reykjavik Geothermal internal report No:100028-05.

Hersir, G.P., and Björnsson, A., 1991: *Geophysical exploration for geothermal resources. Principles and applications*. UNU-GTP, Iceland, report 15, 94 pp.

Hersir, G.P., and Árnason K., 2009: Resistivity of rocks. *Paper presented at "Short Course on Surface Exploration for Geothermal Resources", organized by UNU-GTP and LaGeo, Santa Tecla, El Salvador*, 8 pp.

Hersir, G.P., Guðnason, E.Á., and Flóvenz, Ó.G. (2022): Geophysical Exploration Techniques. In: Letcher, Trevor M. (eds.), *Comprehensive Renewable Energy, 2nd edition, vol. 7*. Elsevier, Oxford, 26–79. *Available at: http://dx.doi.org/10.1016/B978-0-12-819727-1.00128-X*

Ingham, M. R., 1988: The use of invariant impedances in magnetotelluric interpretation. *Geophysical Journal,* 92*,* 165–169.

Domra Kana, J. Djongyang, N., Danwe, R., Njandjock Nouck, P., Abdouramani, D., 2015: A review of geophysical methods for geothermal exploration. *Renewable and Sustainable Energy Reviews, 44*, 87-95. Available at: https://www.sciencedirect.com/journal/renewable-and-sustainable-energy-reviews/vol/44/suppl/C

Johnston, J.M., Pellerin, L. and Hohmann, G.W., 1992: Evaluation of Electromagnetic Methods for Geothermal Reservoir Detection. *Geothermal Resources Council Transactions, Vol 16*. pp 241-245

Jupp, D.L.B. and Vozoff , K., 1975: Stable iterative methods for the inversion of geophysical data. *Geophys. J. Roy. Astr. Soc*., 42, 957-976.

Kazmin, V., 1980: Transform faults in the East African Rift system. *Atti Convegni Lincei, 47*, 65-73.

Kebede, S., 2013: Geothermal exploration and development in Ethiopia: Status and Future plan. *Proceedings of Short Course VIII on Exploration for Geothermal Resources*, *organized by UNU-GTP, KenGen and GDC, Lake Naivasha, Kenya*, 35 pp.

Keir, D., Ebinger, C.J., Stuart, G.W., Daly, E., and Ayele, A., 2006: Strain accommodation by magmatism and faulting as rifting proceeds to breakup: Seismicity of the northern Ethiopian rift. *J. Geophysical Research, 111*, 1-17.

Keller, G.V., and Frischknecht, F.C., 1966: *Electrical methods in geophysical prospecting.* Pergamon Press Ltd., Oxford, 527 pp.

Kristmannsdóttir, H., 1979: Alteration of basaltic rocks by hydrothermal activity at 100-300 C. International clay conference 1978. *Elsevier Sci. Publ. Company,* Amsterdam 1979, 277-288.

Lemma Didana, Y., Thiel., S., and Heinson, G., 2014: Magnetotelluric imaging of upper crustal partial melt at Tendaho graben in Afar, Ethiopia. *Geophysical research letters*, 41, 9, 3089-3095. Available at: *https://agupubs.onlinelibrary.wiley.com/doi/full/10.1002/2014GL060000*

Maguire, P.K.H., Keller, R., Klemperer, S.L., Mackenzie, G.D., Keranen, K., Harder, S., O'Reilly, B., Thybo, H., Asfaw, L., Aftab Khan, M., and Amha, M., 2006: Crustal structure of the northern Main Ethiopian Rift from the EAGLE controlled-source survey; a snapshot of incipient lithospheric break-up. In: Yirgu, G., Ebinger, C., Maguire, P.K.H., *The Afar Volcanic Province within the East African Rift System*. Special Publication of the Geological Society, London. 293–306.

Manzella, A., 2007: Geophysical methods in geothermal exploration. Italian National Research Council, International Institute for Geothermal Research, Pisa, 40 pp. Avalable at: https://geothermalcommunities.geonardo.com/assets/elearning/2.1.A_ManzellaGeophysicalGeochemicalMeth.pdf

Minissale A., Corti G., Tassi F., Darrah T.H., Vaselli O., Montanari D., Montegrossi G., Yirgu G., Selmo E., Teclu A., 2017: Geothermal Potential and Origin of Natural Thermal Fluids in the Northern Lake Abaya Area, Main Ethiopian Rift, East Africa. *Journal of Volcanology and Geothermal Research* 336: 1–18. Avalable at: *http://dx.doi.org/10.1016/j.jvolgeores.2017.01.012.*

Naidu, G.D., Veeraswamy, K., Harinarayana, T., 2011: Electrical signatures of the Earth's crust in central India as inferred from Magnetotelluric study. *Earth Planets and Space 63*, 1175-1182.

Niasari, S.W., 2016: A short introduction to geological strike and geo-electrical strike. *Proceedings of the 1st international conference on Science and Technology.* Published Online, website: *https://doi.org/10.1063/1.4958531*

Park, S.K., and Livelybrook, DW., 1989: Quantitative interpretation of rotationally invariant parameters in magnetotellurics. *Geophysics,* 54, 1483–1490.

Parkinson, W.D., 1983: *Introduction to geomagnetism*. Scottish Academic press, London, 433 pp.

Pellerin, L., and Hohmann, G.W., 1990: Transient electromagnetic inversion: A remedy for magnetotelluric static shifts. *Geophysics, 55-9,* 1242-1250.

Pellerin, L., Johnston J.M., Hohmann G.W., 1996: A numerical evaluation of electromagnetic. methods in geothermal exploration. *Geophysics. 61*, 121-130.

Phoenix Geophysics, 2009: *Data processing. User's guide.* Phoenix Geophysics, Ltd., Toronto.

Quist, A.S., and Marshall, W.L., 1968: Electrical conductances of aqueous sodium chloride solutions from 0 to 800°C and at pressures to 4000 bars. *J. Phys. Chem., 72,* 684-703.

Rangabayaki, R.P., 1984: An interpretive analysis of magnetotelluric data. *Geophysics, 49*, 1730-1748.

Samrock, F., Kuvshinov, A., Bakker, J., Jackson, A., and Fisseha, S., 2015: 3-D analysis and interpretation of magnetotelluric data from the Aluto-Langano geothermal field, Ethiopia. *Geophysical Journal International, 202,* 1923-1948.

Samrock, F., Grayver A.V., Eysteinsson, H., Saar M.O., 2018: Magnetotelluric image of trancrustal system beneath the Tulu Moye geothermal prospect in the Ethiopian rift. *Geophysical research letters, vol 45, issue 23,* 12, pp 847-12.855.

SOHO, 2010: *Solar wind.* Solar and Heliospheric Observatory, website: *http://sohowww.nascom.nasa.gov/gallery/images/magfield.html.*

Simpson, F., and Bahr, K., 2005: *Practical magnetotellurics*. Cambridge University Press, Cambridge, UK, 270 pp.

Stamps, D.S., Calais, E., Saria, E., Hartnady, C., Nocquet, J.M., Ebinger, C.J., and Fernandes, R.M., 2008: A kinematic model for the East African Rift. *Geophysical Research Letters, vol. 35,* 6.

Sternberg, B.K., Washburn, J.C., and Pellerin, L., 1988: Correction for the static shift in magnetotellurics using transient electromagnetic soundings. *Geophysics, 53-11,* 1459-1468.

Swift Jr., C.M., 1967: A *magnetotelluric investigation of an electrical conductivity anomaly in the southwestern United States.* Ph. D. thesis, Massachusetts Institute of Technology, USA.

Teklemariam, M., 2005: Geothermal exploration and development in Ethiopia. *Proceedings of the World Geothermal Congress 2005, Anatalya, Turkey*, 24-29.

Teklemariam, M., and Beyene, K., 2005: Country update on geothermal energy in Ethiopia. *Proceedings in the World Geothermal Congress, WGC 2005*, Antalya, Turkey.

Wiese, H., 1962: Geomagnetische Tiefentellurik Teil II: Die Streichrichtung der untergrundstrukturen des elektrischen Widerstandes, erschlossen aus geomagnetischen Variationen. *Geofisica pura e applicata*, 52, 83-103.

Whaler, K., Hautot, S., 2006: Magnetotelluric studies of the northern Ethiopian rift In: Yirgu, G., Ebinger, C., Maguire, P. (Eds.), The afar volcanic province within the East African Rift System. Special Publication of the geological society, London, p.293-306.

Zhdanov, M.S., and Keller G.V., 1994: *The geoelectrical methods in geophysical exploration.* Elsevier Scientific Publishing Co., The Netherlands, 873 pp.